CHAPTER 1

INTRODUCTION

1.1 Background

Normal concrete is a construction material basically composed of cement (commonly Portland cement), aggregate and water. This type of concrete is admirably suitable for general concrete construction when there is no exposure to severe condition. All the ingredients solidify and harden after mixing with water due to a chemical process known as hydration. The water reacts with the cement, which bonds the other components together, eventually creating a stone-like material. With the increased of knowledge, there are inorganic materials that also have pozzolanic or latent hydraulic properties that can enhance the properties of concrete. These very fine-grained materials are added to the concrete mix as mineral admixtures or as a replacement for Portland cement (blended cements).

Cement replacement material (CRM) is use as a substitute for some of the Portland cement in a concrete. Several types of cement replacement materials are in common use, some of which are by-product from other industrial processes and hence their use may have economic advantages. However, the main reason for their use is that they can give a variety of useful of enhancement of or modifications to the concrete properties. Nevertheless, the use of by-product can reduce the human's carbon footprint which is the most essential step that must take to end overshoot and live within the means of planet.

The carbon footprint is the total set of greenhouse gas (GHG) emissions caused by an organization, event or product and it is most rapidly-growing component. In concrete industry, the production of 1 ton of cement releases about 1 ton of carbon

dioxide in the atmosphere, currently more than 2.5 billion ton of cement is produced yearly all over the world annually. Modern construction of reinforced concrete structures demands the use of high strength and performance concrete. It increases the consumption of cement that will results in high emission of greenhouse gases.

The utilization of the agricultural residue such as rice husk ash, as partial replacement of cement is a new trend in concrete technology in this century. Besides, as far as the sustainability is concerned, it will also help to solve problems otherwise encountered in disposing of the wastes. Together with renewable energy technologies, it offers the promise of a sustainable energy future as world seeks to improve the quality of life for present citizens and future generations alike.

1.2 Problem Statement

Rice covers 1% of the earth's surface and is a primary source of food for billions of people. The annual world production of rice amounts to estimated around 400 million tons of which more than 10% is husk [1]. Globally, approximately 600 million tons of rice paddies are produced every year. On average 20% of the rice paddy is husk, giving an annual total production of 120 million tons [2]. India is a major rice producing country, and the husk generated during milling is mostly used as a fuel in the boilers for processing paddy, producing energy through direct combustion and/or by gasification. Consequently, it is reported that 20 million tons of rice husk ash (RHA) is produced annually.

In Malaysia, there are increased pattern of paddy production in meets the need. As the country develops, the total demand for paddy is expected to increase rapidly resulting in a gradual increase in the marginal economic cost of rice production, particularly in areas where rice production are in short supply as compared to the demand. Table 1.1 shows the Malaysian rice production. As shown in the Table 1.1, the production of husk increased as paddy production increased. As a result, not only in Malaysia, but also in the majority of rice producing countries, much of the husk that produced from the processing of rice either burnt or dumped incurring high waste.

Many of the developing countries produce huge quantities of agro residues but unproductive and inefficiently handling these residues causing extensive pollution to the environment. Apart from the problems of transportation, storage, and handling, directs burning of loose biomass in conventional grates is associated with very low thermal in efficiency and widespread air pollution. Furthermore, this RHA is a great environmental threat causing damage to the land and the surrounding area in which it is dumped.

Table 1.1 Malaysian Rice Production [3]

	2005	2006	2007	TOTAL
Paddy Produced (MT)	1,772,844	1,786,096	1,724,746	5,283,686
Paddy Area (Hectare)	298,453	299,993	292,021	890,467
Avg. Production per Hectare	5.94	5.95	5.91	5.93
Estimated Rice Produced	1,063,706	1,071,658	1,034,848	3,170,212
Husk (MT)	496,396	500,107	482,929	1,479,432

Therefore, commercialization of RHA is an intelligent approach to reduce cost of disposal problem. In addition, the ash contains about 95% pure silica, and, if properly prepared, it is in an active form which behaves very like cement [3]. Even though some of existing practice of burning rice husk produce ash with high silica contain [4], but there is no commercialization of RHA since its only restrict to a lab scale and it is just a few study on the interfacial transition zone problem for rice husk ash concrete. Despite the fact that ash produced from rice husk burning contains high of silica amount [4], the existing burning procedures are not taking into account on the CO_2 released from the burning process.

This study is addressing the issue of carbon footprint and also the right burning procedure to produce a quality RHA and explore more on the interfacial transition zone issues. To such an extent, the utilization of RHA not only solves the rice husk disposal problem but generates substantial savings associated with the energy costs of the rice mill: reduction of power consumption from the grid and substitution of oil as fuel for paddy drying.

1.3 Objectives

The main purposes of the research are to:

1) Establish the best burning temperature and burning method for optimal output of MIRHA in terms of SiO_2 quantity and quality.
2) Determine the effect of MIRHA on compressive strength, porosity and interfacial transition zone characteristic of concrete.

1.4 Scope and Limitation of Study

This laboratory investigation was carried out within the scope as stated below:

1. The effect of microwave incinerated rice husk ash (MIRHA) and rice husk ash (RHA) on:
   a. Concrete compressive strength (150 mm cube sample)
   b. Concrete porosity (50 mm Ø x 40 mm cored sample)
   c. Interfacial zone characteristic
      i- Aggregate/Mortar bonding (30 mm Ø x 30 mm high)
      ii- Thickness of interface (10 mm Ø x 2 mm high slice)
2. Three types of RHA used in this study is shown in Table 1.2:

Table 1.2 Types of RHA

Types of RHA	Method Of Burning	Place Obtained	Temperature Of Burning
MIRHA (Microwave Incinerated Rice Husk Ash)	Microwave Incinerator	UTP	a) 800°C b) 700°C c) 600°C
SGR-RHA (Sg. Ranggam Rice Husk Ash)	Boiler	Sg. Ranggam, Perak	600°C - 900°C
SGM-RHA (Sg. Manik Rice Husk Ash)	Cyclonic Husk Furnace	Sg. Manik, Perak	1000°C

3. MIRHA, SGR-RHA and SGM-RHA were incorporated as a partial cement replacement material at 5%, 10%, 15% and 20%.

4. X-Ray Diffraction (XRD) and X-Ray Fluorescence (XRF) were used to analyze the material composition of MIRHA, SGR-RHA and SGM-RHA.
5. Analysis of concrete characteristic namely their:
    - Compressive strength test at ages 3, 7, 28 and 56 days – three samples.
    - Porosity test at 28 days – three samples.
    - Interfacial zone characteristic test at 28 days consist of push-out test and Scanning Electron Microscope (SEM) test – three samples.

1.5 Schematic Flow Chart of the Methodology

This laboratory investigation was carried out within the scope as stated in Figure 1.1 below:

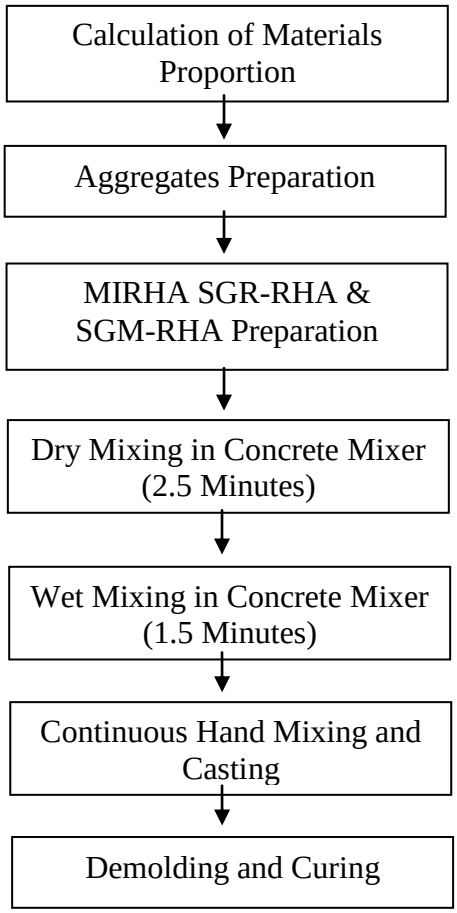

Figure 1.1 Process Flowchart of Sample Preparation.

CHAPTER II
LITERATURE REVIEW

2.1 Properties of Rice Husk Ash (RHA)

The utilization of the agricultural residue such as rice husk ash (RHA), as cement replacement is a new trend in concrete technology in this century. Besides, as far as the sustainability is concerned, it will also help to solve problems otherwise encountered in disposing of the wastes. Many uses of RHA have been proposed depends on the properties of RHA. Dry rice husk is collected when paddy is threshed to separate the rice and husk. Extensive research carried out [5, 6, 7] revealed that the ratios of rice husk in paddy varies from about 16 to 25 wt.% of the paddy while the ash content varies from about 13 to 30 wt.%.

2.1.1 Mineral

To be categorized as a true mineral, a particular kind of material must be a firm and stable in shape and have a crystalline structure which has been formed as a result of geological processes. The material must also be a naturally occurring, homogeneous substance with a defined chemical composition.

RHA has been categorized as a mineral due to its structure and chemical composition. It has been established from previous research, that wide range of chemical composition of rice husk existed ash depends on the source subjected to location, climate, etc. The chemical composition of rice husk is similar to that of many common organic fibres. Table 2.1 shows the mineral composition of rice husk that has been investigated by previous researchers. The holocellulose (cellulose combined with hemi cellulose) content in rice husk is about 54%, but the chemical

composition of ash and lignin after burning differ slightly depending on the species [8, 9].

Table 2.1 Mineral Composition of Rice Husk [8, 9].

Content	Type of polymer
Cellulose ($C_5H_{10}O_5$)	glucose
Lignin ($C_7H_{10}O_3$)	phenol
Hemi cellulose	xylose
SiO_2	primary component of ash

The properties of rice husks after burning are similar to silica fume in that SiO_2 content is about 90% to 95% [10, 11]. Based on previous study of burnt husk or ash, the general analysis shows a silica content of 79.5 to 97.6 wt.% [5, 12, 13]. There is an analysis of husk that discloses the presence of cellulose, hemicelluloses mainly as pentosans, lignin, water, proteins and fats, small amounts of vitamins and acids [14]. Preceding research also found that cellulose and pentosans make up nearly 50 to 60 wt.% of the husk but besides this, the chemical composition is indeterminate [5, 6, 15]. Lignin content is different and it ranges between 20 and 45 wt.%. An average ash content of 20 wt.% of the total dry weight of rice husk is counted as a reasonable approximation.

Houston [5] earlier reports on American and Spanish rice husk ash indicates K_2O contents of 0.58 to 2.5% in ash. Meanwhile the K_2O in rice husk ash obtained from a boiler using rice husk as fuel in Eastern India was found to be 1.09 wt.% [16]. The phosphate content of rice husk is of importance in cement applications. It is due to the effect of phosphate as inorganic retardant act as a water reducer. Phosphate content varies from a low 0.2 to a high 2.85 wt.% P_2O_5 in ash [5]. Whereas the ash from Eastern India contains 0.54 wt.%. Obviously low soda, potash and phosphate contents would be preferred for use as a cement admixture.

2.1.2 Silica

Rice husk contains nearly 20% silica, which is present in hydrated amorphous form [13]. On thermal treatment, silica will convert to crystalline form which is known as crystobalite. Rice husk ash can comprise a very high percentage of crystalline silica [13]. The silica in rice husk ash itself is considered to be opaline, glassy, or gel like. There is no uncertainty that the silica is occurring in a hydrated form within the raw husk and is generally believed to be transported in the paddy plant as monosilicic acid [14]. At the husk surface, this acid eventually polymerises to form a cellulose-silica membrane. As stated by Jauberthie et. Al [17], the external face of the husk shows a high concentration of silica, much weaker on the internal face and virtually non-existent within the husk. A detail examination of these zones is set out in Tables 2.2-2.4. These consequences confirm that the presence of amorphous silica is concentrated at the surfaces of the rice husk and not within the husk itself.

Table 2.2 Micro Analysis of the External Surface of the Rice Husk [17]

Element	% (by weight)	% (atomic)
C	6.91	11.11
O	47.93	57.84
Si	45.16	31.05
Total	100.00	100.00

Table 2.3 Micro Analysis of the Interior Surface of the Rice Husk [17]

Element	% (by weight)	% (atomic)
C	62.54	69.54
O	35.19	29.38
Si	2.27	1.08
Total	100.00	100.00

Table 2.4 Micro Analysis of the Inner Surface of the Rice Husk [17]

Element	% (by weight)	% (atomic)
C	30.20	40.93
O	42.53	43.27
Si	27.27	15.08
Total	100.00	100.00

According to these tables, it shows that the rice husk and the rice husk ash comprise strong concentration of silica exist in a crystalline (quartz) and amorphous

forms. It is found that on the external face of the husk the amorphous silica occurs principally and it is lesser concentration on the inner surface. This circumstance explains the pozzolanic role.

2.1.3 Amorphousness

Amorphous silica rice husk is burnt in controlled temperatures below 700°C. The ash generated is amorphous in nature. It has been reported that the highest amount of amorphous silica could be found in samples burnt in the range of 500°C - 700°C [4] meanwhile another researcher stated that a highly reactive ash could be produced by maintaining the combustion temperature below 500°C [1].

It also has been detailed by Hamad [18] that ash prepared at a temperature of about 500°C to 600°C consisted of amorphous silica. The amorphous state could be achieved with under oxidising conditions for relatively prolonged period or up to 680°C, provided that the high temperature exposure was less than one hour. The transformation of this amorphous state to crystalline state takes place if the ash is exposed to high temperatures of above 850°C. The silica was predominantly in amorphous form that the crystals present in the ashes grew with time of burning for incineration temperature up to 700°C [19].

2.1.4 Crystallinity

It is not recommended to burn rice husk above 800°C longer than one hour, because prolonged heating above this temperature may cause the material to convert (at least in part) to crystalline silica; first to cristobalite and then tridymite [4]. At 800°C, the ash will convert to cristobalite and after burning at 1150°C both cristobalite and tidymite will be formed. This crystalline are unable to react with $Ca(OH)_2$ to form calcium silicate hydrate (C-S-H) gels which is a vital process for concrete better performance.

2.1.5 Pozzolanic Material

Pozzolana as defined by ASTM C 618 [20] is a material which is siliceous or siliceous and aluminous material by composition. In general, pozzolana has little or no cementitious value, however, in finely divided form and in the presence of moisture, it can react with $Ca(OH)_2$ at room temperature to provide cementing property [21]. When pozzolans are used in combination with portland cement, $Ca(OH)_2$ set free from the hydration of cements, reacts with the aluminosilicates in the pozzolans to form cementitious compounds possessing cohesive and adhesive properties [22].

In the concrete industry, a common adage is that there are two guarantees. One, it will get hard and two, it will crack. Cracking cannot be prevented but it can be significantly reduced or controlled when the causes are taken into account and preventative steps are taken. This concrete problem can be minimized by using pozzolanic materials due to the expansive gels formed by the alkali silica reaction [13]. In concrete, these highly active pozzolans are recently utilized as Cement Replacement Material (CRM). Ramachandran in Table 2.5 shows the general classification of mineral admixture with specified chemical and mineralogical composition and particle characteristics [23]. As stated by this general classification, RHA has been classified as highly active pozzolan.

Table 2.5 Classification of Mineral Admixtures [23].

Classification	Chemical and Mineralogical Composition	Particle Characteristics
II. Highly active pozzolans		
a. Condensed silica fume	Consists essentially of pure silica in non crystalline form	Extremely fine powder consisting of solid spheres of 0.1 μm average diameter (about 20 m^2/g surface area by nitrogen adsorption).
b. Rice husk ash; (Mehta-Pitt process)	Consists essentially of pure silica in non crystalline form	Particles are generally less than 45 μm but they are highly cellular (about 60 m^2.g surface area by nitrogen adsorption
III. Normal pozzolans		
a. Low calcium fly ash	Mostly silicate glass containing aluminium iron, and alkalies. The small quantity of crystalline matter present consists generally of quartz, mullite, silimanite, hematite, magnetite	Powder corresponding to 15-30% particles larger than 45 μm (usually 200-300 m^2/kg Blaine). Most particles are solid spheres of average 20 μm diameter. Cenospheres and plerospheres may be present.
b. Natural materials	Besides aluminosilicates glass, natural pozzolans contain quartz, feldspar, mica.	Particles are ground to mostly under 45 μm and have rough texture.
V. Normal pozzolans		
Slowly-cooled blast furnace slag, bottom ash, boiler slag, field-burnt rice husk ash.	Consists essentially of crystalline silicate minerals and only a small amount of non crystalline matter.	The materials must be pulverised to very fine particle size in order to develop some pozzolanic activity. Ground particles are rough in texture.

2.2 Burning of RHA

The quality of RHA also depends upon the preservation of cellular structure and the extent of amorphous material within structure [8]. Burning temperature, time, and environment, have different effects to the RHA produced.

2.2.1 Temperature

Under controlled burning in terms of temperature conditions, amorphous silica with high reactivity, ultra fine size and large surface is produced. However, the amorphous silica is highly reactive in nature. Previously, Hamad and Khatab [16] have observed that the ash formed at lower temperatures (500°C-600°C) consisted of amorphous silica. The crystalline forms namely cristobalite and trydimite were detected at temperatures greater than 800°C and greater than 1200°C respectively.

The ash produced by combustion of rice husk in a fixed bed at different air rates was also evaluated. At lower rates of combustion, amorphous silica was formed whereas at higher rates, silica crystallized. Crystallisation of silica has to be prevented by controlling the temperature and time of burning so that maximum amorphous variety is produced. Milling the ash to get high surface area can increase the reactivity. Table 2.6 shows the chemical composition of RHA under different burning temperatures.

SiO_2 content will be increased by burning the RHA with higher temperature. But it is not suggested to burn rice husk above 800°C longer than one hour, because it tends to cause a sintering effect (coalescing of fine particles) and is indicated by a dramatic reduction in the specific surface [8]. Khalaf et al. [24] found out that when the husk was converted to ash by uncontrolled burning below 500°C, the ignition was not completed and considerable amount of left burnt-carbon was found in the resulting ash. Carbon content in excess of 30% was expected to have an adverse effect upon the pozzolanic of RHA [25]. The ash produced by control burning of the rice husk between 550°C and 700°C incinerating temperature for 1 hour transform the silica content of the ash into amorphous phase [26, 27].

The reactivity of amorphous silica is directly proportional to the specific surface area of ash [28].

Table 2.6 Chemical Composition of RHA under Different Burning Temperatures [10]

		Temperature (°C)				
		<300	400	600	700	1000
Element (%)	Si	81.90	80.43	81.25	86.71	92.73
	K	9.58	11.86	11.80	7.56	2.57
	Ca	4.08	3.19	2.75	2.62	1.97
	Na	0.96	0.92	1.33	1.21	0.91
	Mg	1.25	1.20	0.88	0.57	0.66
	S	1.81	1.32	1.30	1.34	0.16
	Ti	0.00	0.00	0.00	0.00	0.45
	Fe	0.43	1.81	0.68	0.00	0.68
Oxide (%)	SiO_2	88.01	88.05	88.67	92.15	95.48
	MgO	1.17	1.13	0.84	0.51	0.59
	SO_3	1.12	0.83	0.81	0.79	0.09
	CaO	2.56	2.02	1.73	1.60	1.16
	K_2O	5.26	6.48	6.41	3.94	1.28
	Na_2O	0.79	0.76	1.09	0.99	0.73
	Fe_2O_3	0.29	0.74	0.46	0.00	0.43

2.2.2 Duration

Longer burning time will cause collapse of the cellular form and also coalescence of the fine pores [10], which consequently causes a reduction in surface area [10]. Combustion environment also plays an important role. It should be noted that a change in the rate of oxidation from moderately oxidizing conditions (CO_2 environment) to highly oxidizing conditions (oxygen environment) is responsible for the steep drop in the micro porosity and surface area [8]. The effect of the combination of various conditions to RHA is shown in Table 2.7.

Table 2.7 Effect of Burning Conditions on the Crystal Structure and Surface Area of Rice Husk Ash. [29].

Burning Temperature (°C)	Hold Time	Environment	Properties of ash	
			Crystalline	Surface Area (m^2/g)
500-600	1 min	Moderately oxidizing	Non crystalline	122
	30 min			97
	2 hours			76
700-800	15 min – 1 hr	Moderately oxidizing	Non crystalline	100
	> 1 hour	Highly oxidizing	Partially crystalline	6-10
> 800	> 1 hour	Highly oxidizing	Crystalline	< 5

At higher temperatures with longer burning times, a crystalline structure is formed with a sharp reduction in surface area. This lowers the pozzolanic activity. Figure 2.1 indicates the ideal time/temperature path to obtain optimum quality rice husk ash with a microporous and cellular structure which is highly reactive [8].

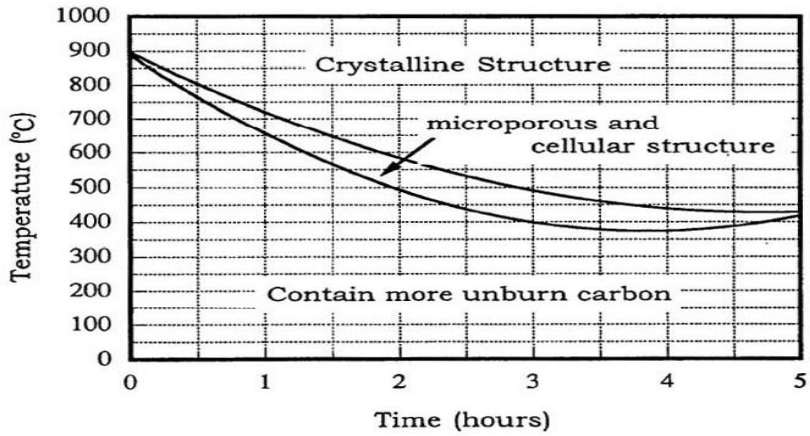

Figure 2.1 The Optimum Incineration Condition Curve for Obtaining Reactive Cellular RHA [8].

2.2.3 Method of Burning RHA

RHA obtained from burning process of paddy husk is one of the cement replacement materials produced from agriculture waste. These materials are generally a waste by-product and contain highly reactive silica to react with calcium hydroxide resulted from hydration process between cement and water. The process of making ash from rice husk specifically for the purpose of pozzolana production would result in a loss of this energy. Many processes have been developed to form rice husk specifically for use as an admixture in cements. Techniques for useful burning of ash to produce pozzolana quality material have been developed and are well documented [30].

2.2.3.1 Heap Burnt

Heap burning is an easy technique of reducing the husk to ash. It is conducted in an enclosed compound and the burning husk is raked from time to time to provide a white to white-black ash. Plentiful air should be available even temperatures in this method would obviously vary from location to location. This can be ensured if raking is done carefully. Heap burning is carried out in a 16m diameter circular compound made with brick and in this burning method, about 2.5m high piles of husk is made [29].

2.2.3.2 Oven / Boiler Beds

Burning in ovens or in boiler beds leads to white and white-black ash [14]. Sometimes there is impassioned over burned leading to crystallization of silica because there is a wide variation in carbon content due to the accessibility of air within the oven or boiler [14]. Burning in ovens and from boilers used for parboiling or rice does not permit much control on burning temperature.

The ash from such boilers and ovens has the advantage of being available in large quantity at a single place [14]. Secondly, there is a regular output of ash in such boiler or oven units where rice husk is used as a fuel. Most importantly, ash produced in boiler and ovens are those in which the energy stored in rice husk is utilized usefully

to produce heat for other applications [14]. The quality of ash expected from various burning process is given in Table 2.8 [31].

Table 2.8 Nature of Ash from Various Burning Processes [31].

Types of Process	Ash Product
Heap Burnt	Crystalline Cristobalite
Oven Burnt	Amorphous Product + Crystalline Cristobalite
Brick Stove	Amorphous Product + Crystalline Quartz (minor)
TiB2 Stove	Amorphous Product + Crystalline Quartz (minor)
Downdraft Kiln	Crystalline Trydymite

2.2.3.3 Cyclonic Husk Furnace (CHF)

A horizontal cyclone furnace was designed [32] and developed for combustion in the mill and the energy was used for par boiling and drying paddy. The ash produced did not contain any volatile matter but some traces of unburnt carbon.

The cyclonic husk furnace is the source of the hot air supply to the dryers. The furnace produces hot clean air environment friendly and reduces energy costs by the replacing the oil burner and gas fired furnaces. High efficiency in combustion according to double cyclonic system which create an air/husk vortex to make a completely combustion-release smokeless has produced a clean hot air and friendly environment. The spiraling vortex of air forces ash fall to the bottom with special cooling system 35°C temperature of touchable ash reduce no water necessary. Auto controlled husk feeder by a variable speed inverter with pit control ensure regular and even hot air supply minimum time delay between start up and actual operation (temperature increase from 0°C to 150°C within 10 minutes) [33].

2.2.3.4 Boiler

In general, rice husk is the only fuel used in the boiler. During this process, ash is continuously evacuated from the boiler and stored. A programmable logic controller (PLC) provides fully automatic monitoring, process control, safety control and alarm feedback when necessary, for the boiler system. The back pressure turbine converts the thermal energy available in the form of steam into mechanical energy (shaft power) and the generator converts the mechanical energy into electrical energy. Compared with other solid fuels, rice husk has very high ash content and is quite abrasive. The boiler generates superheated steam at 30 bar and 300 degrees Celsius [34].

The boiler steam pressure is a major determinant of efficiency and power output of the cogeneration system. Generally, higher steam pressure is desirable because the enormous energy extraction and higher efficiencies. However, high steam pressures may cost significantly more, may require more stringent water purity specifications, and may need much more qualified staff to operate and maintain. Steam turbines transform available heat in the steam into kinetic energy and utilize steam velocity to induce torque upon a rotor. This system is used to provide direct heat for drying paddy rice in continuous flow vertical column dryers and flat bed dryers. System input heat release is 12.0 mm BTU/hr. Addition of boiler, turbine/generator and auxiliaries for generation of 225 kW of electricity. Boiler exhausts heat used for paddy rice drying [35].

2.2.3.5 Microwave Incinerator

Nowadays, industries that have drying process in production prospect, i.e. paper industries, printing industries, and leather industries mostly use microwave heating in their processes. One of the most interesting industrial applications also involves the use of microwaves to generate extreme internal stresses in rock and concrete to “crush” the material for removal or disposal. One industrial application that results in superior material quality with microwave heating is the sintering of ferrite and ceramic materials.

Sintering involves applying pressure and heat to a mould filled with granular or powdered material to cause the grains fuse together into a solid part [36]. In food services and agriculture industries, this type of heating was employed frequently which it was found that microwave energy couples very well with water molecules. They are present in large quantities in most food products and vegetable matter. In addition, it was realized early on that microwaves are useful in dehydrating, cooking, thawing, freeze drying, and the destruction of fungus, yeast, bacteria, mildew, and pests from many food products. The spoiling of certain fruit and vegetable products can be reduced or delayed through enzymatic inactivation by microwaves [36].

It has been identified, appropriate burning method can give a great effect in producing RHA with high reactivity of silica as it can significantly enhance the concrete properties. Apart from that, microwave incinerator which is a modern incinerator, is designed to avoid environmental problem as caused by open burning. It is the one of the modern incinerators that proposed to produce amorphous MIRHA with high pozzolanic reactivity. Therefore, a special microwave incinerator is bought by Universiti Teknologi Petronas not only to have a proper burning process but also can produce RHA with great quality. These microwaves are part of the electromagnetic spectrum and are located between 300 MHz and 300 GHz. Microwave heating is defined as the heating of a substance by electromagnetic energy operating in that frequency range [37].

There is a fundamental difference in the nature of microwave heating when compared to conventional methods of heating material. Conventional heating relies on one or more of the heat transfer mechanisms of convection, conduction, or radiation to transfer thermal energy into the material. In all three cases, the energy is deposited at the surface of the material and the resulting temperature gradient established in the material causes the transfer of heat into the core of the object. Thus, the temperature gradient is always into the material with the highest temperatures being at the surface [36].

It is found that, in microwave heating, the microwave energy not only interacts with the surface material but also penetrates the surface and interacts with the core of

the material as well. Energy is transferred from the electromagnetic field into thermal energy throughout the entire volume of the material that is penetrated by the radiation. Microwave heating does not rely on conduction from the surface to bring heat into the core region. Since the heating rate is not limited by conduction through the surface layer, the material can be heated quicker [36]. Another important aspect of microwave heating is that it results in a temperature gradient in the reverse direction compared to conventional heating. That is to say, the highest temperature occurs at the centre of the object and heat is conducted to the outer layer of the material [36]. Schematic diagram of the comparison between conventional heating and microwave heating can be seen as illustrated in Figure 2.2.

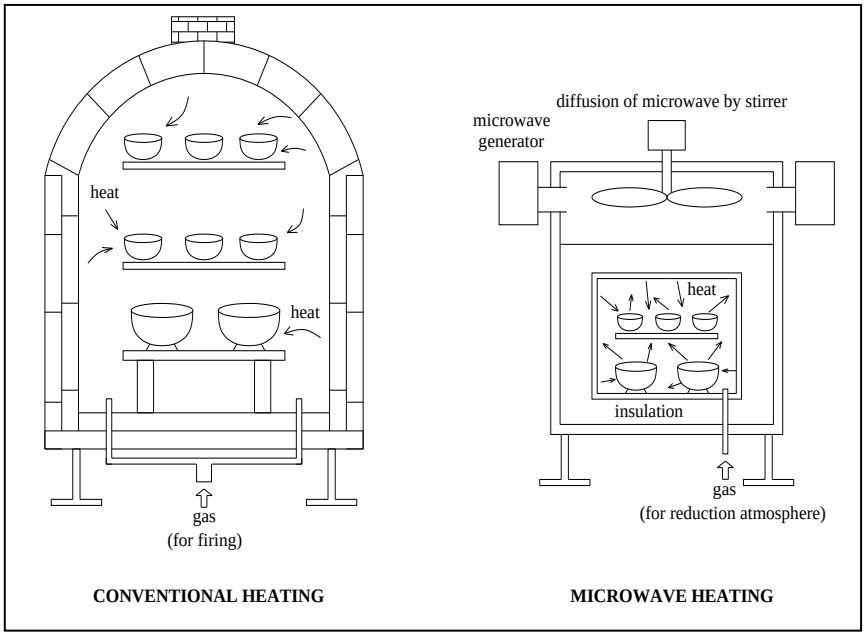

Figure 2.2 Comparisons of Conventional Heating and Microwave Heating [38].

Since the heating rate is not limited by the conduction through the surface layer, material can be heated quicker with microwave heating. The shorter process time gives economical advantages to the whole production process. Problems such as cracking that may occur when drying material (during drying material or when material dried) can be reduced, because the heat is generated in all parts of the material that are receiving radiation.

This effect reduces the internal stresses in the material and can help eliminate cracking that may occur when the internal stresses become too large [36]. The most important matter of this incinerator is the additional device called Flue Gas Filter that equipped to the microwave incinerator and provide significant positive effect to the environment. It can distil all the dust and ashes that are resulted from rice husk incineration, hence the air pollution from burning process can be reduced [36].

2.2.4 Type of Test of RHA Characteristic

2.2.4.1 X-Ray Fluorescence (XRF)

X-Ray Fluorescence (XRF) is an analytical technique that uses the interaction of x-rays with a material to determine its elemental composition. XRF is suitable for solids, liquids and powders, and in most circumstances is non-destructive. XRF is widely used as a fast characterization tool in many analytical laboratories across the world, for applications as diverse as metallurgy, forensics, polymers, electronics, archaeology, environmental analysis, geology and mining. Recent advances in X-ray technology have led to the development of XRF instruments capable of high spatial resolution analysis, which are now embraced by researchers and analysts within these application areas.

XRF is named as the process of emissions of characteristic x-rays. When a primary x-ray excitation source from an x-ray tube or a radioactive source strikes a sample, the x-ray can either be absorbed by the atom or scattered through the material. The process in which an x-ray is absorbed by the atom by transferring all of its energy to an innermost electron is called the "photoelectric effect" [37]. During this process, if the primary x-ray had sufficient energy, electrons are ejected from the inner shells, creating vacancies. These vacancies present an unstable condition for the atom. As the atom returns to its stable condition, electrons from the outer shells are transferred to the inner shells and in the process give off a characteristic x-ray whose energy is the difference between the two binding energies of the corresponding shells. Because each element has a unique set of energy levels, each element produces x-rays at a unique set of energies, allowing one to non-destructively measure the elemental composition of a sample.

Analysis using x-ray fluorescence is called "X-ray Fluorescence Spectroscopy" [39] and referring to BS EN 12677 [40] for the standard of test. Figure 2.3 reveals that when a radiation from x-ray tube or radioisotope coming, an electron in the K shell is ejected from the atom by an external primary excitation x-ray, creating a vacancy. An electron from the L or M shell "jumps in" to fill the vacancy. In the process, it emits a characteristic x-ray unique to this element and in turn, produces a vacancy in the L or M shell. This process allows a measurement of elemental composition of a sample [39].

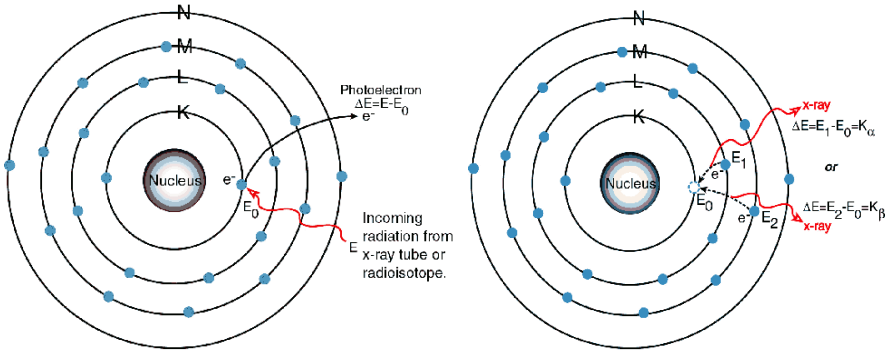

Figure 2.3 X-Ray Fluorescence Process [39].

In some of study [41], XRF is usually used to analyze the chemical composition of a material. Deep comprehension into the chemical composition of the tested material will provide better description to the research outline and analysis. Table 2.9 shows the chemical composition of ordinary Portland cement (OPC), rice husk ash (RHA), and silica fume (SF) that have been investigated by former researchers.

Table 2.9 Chemical Compositions of OPC, RHA, and SF [31]

	SiO_2	Al_2O_3	Fe_2O_3	CaO	MgO	Na_2O	K_2O	P_2O_5	TiO_2	SO_3	C	Cl
OPC	20.1	4.51	2.50	61.3	3.13	0.24	0.39	<0.9	0.24	4.04	-	-
RHA	87.2	0.15	0.16	0.55	0.35	1.12	3.68	0.50	0.01	0.24	0.45	5.91
SF	93.6	0.06	0.45	0.50	0.67	0.16	0.85	0.09	0.01	0.32	-	-

From Table 2.9, it shows that RHA have similar chemical compositions with SF. SiO_2 contents of RHA and SF have not much different and it is believe that RHA have a potential as a pozolanic material.

2.2.4.2 X-Ray Diffraction (XRD)

Routine XRD-mineralogy profiles can provide qualitative and semi quantitative records of shifts in the source of sedimentary components to a late sequence. XRD mainly displays information on autochthonous and authigenic minerals, but can give some indication of the abundance of amorphous silica phases. Set up with routine data collection, XRD is a rapid, accurate technique which can process 40 samples per day using an automated sample changer [42].

Each mineral is defined by a crystal lattice with characteristic diffraction properties resolved by x-rays. The Angstrom d-spacing of certain crystallographic lattice directions show up as relative peak (area) heights on the diffractogram (usually in mm) in a fixed relationship to the 2θ (two-theta) angle of the scintillator counter as defined by Bragg's law of diffraction. Using calibrated peak area intensities of the major peak, the proportion of mineral species in a profile can be given with about ± 5% at least for minerals which constitute more than 5% of the bulk sample. Generally, corundum is used as the reference mineral for intensity and for d-spacing [42].

Figure 2.4 shows that based on Bragg's law, $n\lambda = 2d\sin\theta$, by controlling the wavelength with vary and continuously measure the incident angle, it will leave only the lattice plane spacing as variable. So whenever a constructive interference is observed, at that point a fundamental spacing parameter for the mineral of interest can be calculated [42].

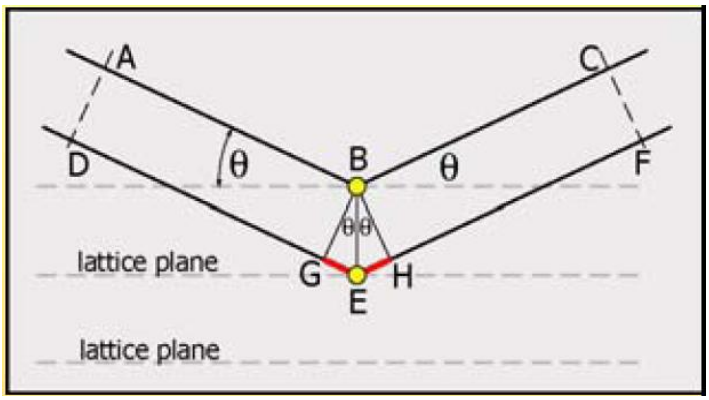

Figure 2.4 Geometry of X-Ray Reflection [43]

The amorphousness degree of material samples can be judged by the intensity or average height of the diffused band between 15° and 26° values of 2θ, using x-rays generated from a copper target and nickel filter [44]. Figure 2.5 shows the XRD result obtained from various samples of RHA. RHA A and RHA B show the amorphous nature of samples, whereas the peaks of quartz could be detected in the other samples. The presence of quartz shown by the XRD of RHA C can be due to the longer duration burning or can also be attributed to the contamination of sand particles from the pit of burning location [45].

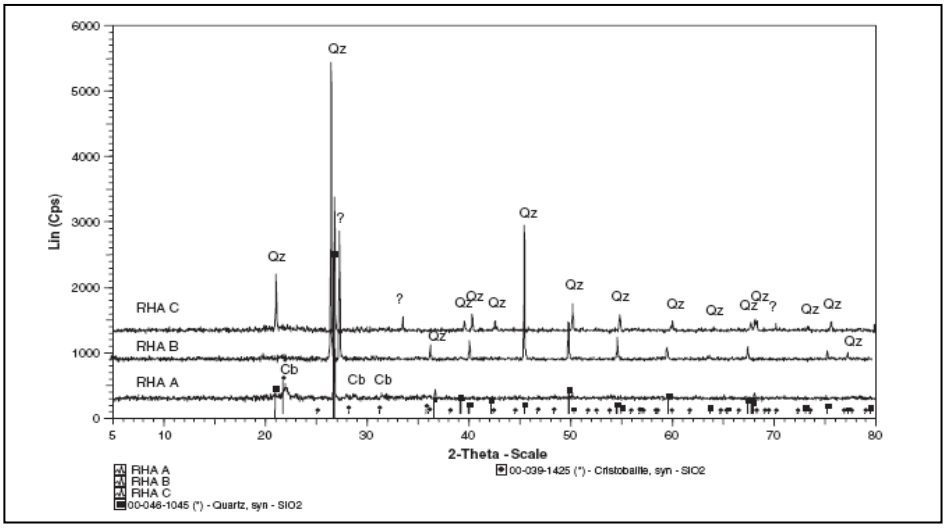

Figure 2.5 XRD Graphs from Various Samples of RHA [45].

2.2.5 Scanning Electron Microscope (SEM)

The Scanning Electron Microscope (SEM) is a microscope that uses electron rather than light to form an image. In optical microscope, lenses are used to bend the light waves and the lenses are adjusted for focus. In the SEM, electromagnets are used to bend an electron beam which is used to produce the images on a screen. Beam of electron is produced in an electron gun by heating of a metallic filament. This electron beam will follow a vertical path through the column of the microscope and pass electromagnetic lenses, which focus and direct the beam towards the sample. When the electron beam hits the sample, other electrons, called as backscattered electron and secondary electron, are ejected from the sample. The detectors will collect these

secondary and backscattered electrons and convert them to a signal that is sent to a display screen [46].

The SEM is designed for direct studying of the surfaces of solid object [46]. In previous researches of rice husk ash material, the SEM was utilized to analyze the surface properties of rice husk ash (RHA) it self and cement paste that incorporating RHA. SEM analysis is carried out to verify the result obtained from another experiments, hence the accuracy of data obtained can be supported. The observation on rice husk ash that has been done by Jauberthie et.al [18] explained the cause of quartz content in RHA. It is said that the origin of the quartz may be attributed to one of or a combination of the following factors: contamination by wind blown sand, transported into the plant by the sap, and crystallisation of the silica at the calcinations temperature [47]. Figure 2.6 shows the characteristic of initial RHA after calcinations [47]. The SEM is also can be used to analyze the presence of C-S-H gels as the product of pozzolanic reaction [48]. Figure 2.7 shows the presence of C-S-H gels in cement paste that incorporating RHA.

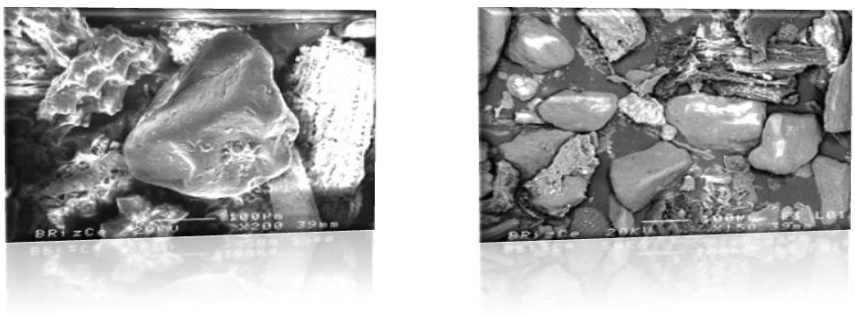

Figure 2.6 SEM Observation of the Rice Husk Ash [47]

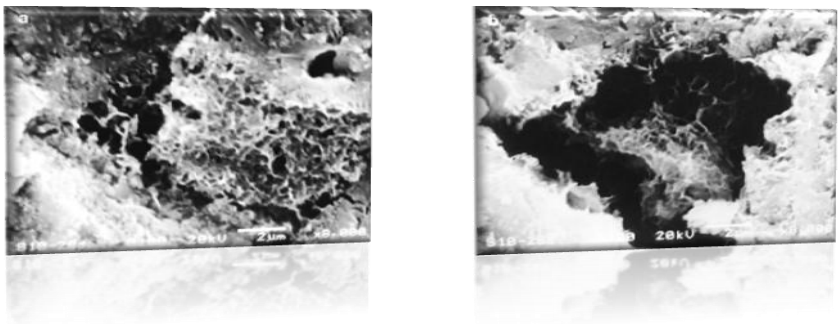

Figure 2.7 SEM Images of C-S-H Gels in the Cement Paste [47]

2.3 Effect of RHA on Concrete Characteristic

2.3.1 Compressive Strength

Several papers [49, 50] have been published on the performance of RHA blended concrete. In the present context, optimal level refers to the maximum favorable percentage of replacement of OPC with RHA up to which the strength and of blended are equivalent or more than that of unblended OPC concrete. Furthermore, as a pozzolanic material, RHA has significantly benefits when utilized in the concrete mixture. High SiO_2 contents in RHA are able to react with $Ca(OH)_2$ to form calcium silicate hydrate (C-S-H) gels and lead to the better performance of concrete properties. This phenomenon is able to promote RHA as a one of potential cement replacement materials.

The addition of pozzolanic material into concrete mixture is known for the ability to improve the concrete strength at late days [37]. As a finding that RHA as a pozzolana with high amorphous silica content also can give a significant attribution in concrete process. The strength increment for concrete with pozzolana is achieved through pozzolanic reaction between SiO_2 in RHA and calcium hydroxide formed by hydration process. Thus, it explains the late progress of pozzolanic concrete. Commonly, pozzolanic concrete will gain strength lower than normal OPC concrete at early days [37]. After pozzolanic reaction takes place and consume calcium hydroxide, the strength of pozzolanic concrete start to get higher and achieve better performance on late days compared to normal OPC concrete. The product of pozzolanic reaction, which is known as C-S-H gels, hold-up the aggregate-cement paste interfaces and fill empty spaces in pore structures [37]. With higher packing density at late days, pozzolanic concrete will provide higher compressive strength than normal OPC concrete [37]. Table 2.10 shows the mix proportions and compressive strength of RHA concrete that incorporating various percentage of RHA.

The consequence of this previous research shows at early days the pozzolanic concrete gain strength lower compared to normal concrete. From the result it can see that after several days, both pozzolanic concrete and normal OPC concrete will

achieve similar compressive strength but pozzolanic concrete will attain superior compressive strength than the normal OPC concrete at late days [50].

Table 2.10 Mix Proportions and Compressive Strength of RHA Concrete [50]

RHA (%)	Mix Proportion (kg/m^3)					Compressive Strength (MPa)			
	C	RHA	C.A	F.A	W	3-d	7-d	28-d	1-yr
0	392	-	1062	786	128	45	56	65	80
9	356	36	1062	786	128	42	56	77	86
0	410	-	1044	786	128	47	60	66	80
13	356	54	1044	786	128	45	60	80	92
0	428	-	1026	786	128	47	62	70	81
17	356	72	1026	786	128	46	65	80	92

2.3.2 Porosity

Concrete porosity is stated in terms of percentage by volume of concrete. The strength and durability of concrete also influence by its porosity characteristic [51]. Many researchers have found that porosity of concrete can be reduced using pozzolana or supplementary cementing material. There are two principal contributing attributes of pozzolana. Firstly, the pore structure in the cement paste matrix can be denser using a quality pozzolan. Secondly, the chemical reactions of lime crystals that form binders increase paste density, reduced porosity over time, and enhance the matrix chemical resistance to many aggressive attacks. Application with the addition of pozzolanic materials, can affect the porosity of concrete by strengthening the aggregate-cement paste through pozzolanic reaction. This phenomenon is shown in Figure 2.8.

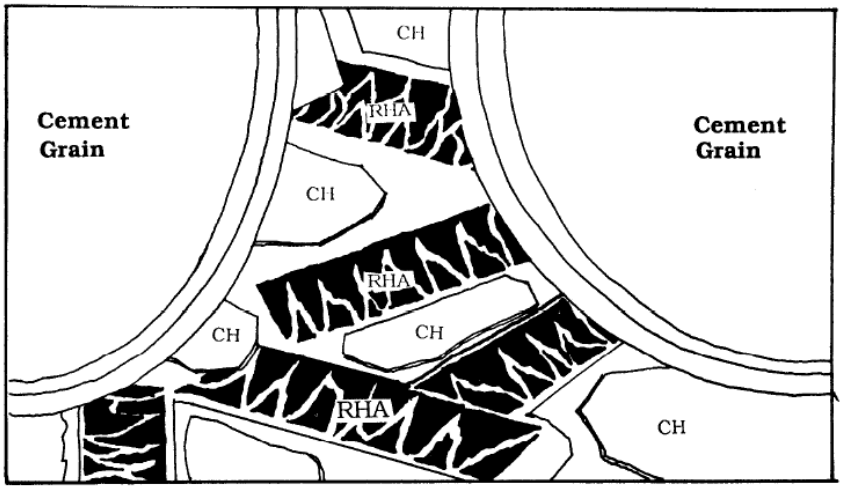

Figure 2.8 Mechanism of Void Filling and Interfacial Transition Zone Strengthening Effect of RHA [8].

It is known that the pozzolanic reaction modifies the micropores structure. Moreover, the products formed due to the pozzolanic reactions occupy the empty spaces in concrete pore structures which thus become sufficiently dense. The porosity of cement paste is then reduced, and as a consequence, the pores are refined. It has shown by researcher [8] that there is a significant reduction in the porosity of cement paste with RHA additions and refinement in the pore structure.

2.3.3 Interfacial Transition Zone.

There are several papers discussed the importance of the cement paste-aggregate interfacial transition zone (ITZ) in influencing concrete properties. Previous researchers has been shown that concrete must still be considered as a three-phase material (paste, aggregate, and ITZ) to properly investigate elastic properties [52, 53], even when air voids are not considered and also on the transport coefficients [54], and drying shrinkage [38]. It is due to the microstructure of the ITZ in ordinary concrete that is different than that of the bulk paste as such need to be considered. It contains more and larger pores and less anhydrous cement and calcium silicate hydrate gel [55, 56]. Effect from that, its response to mechanical and thermal loadings and chemical ingress will also differ from that of bulk paste.

Moreover, it has been stated that the enhanced mechanical properties and reduced permeability of silica fume concrete is believed to be due to the reduction in the thickness of the interfacial zone between the aggregate and paste matrix [57-60]. Due to its extremely fine size and high pozzolanic reactivity, silica fume reduces the porosity, and also the preferential deposition of Ca(OH), in the interfacial zone [61]. Apart from that, study shows the rice-husk ash which has a median particle size of about 7 μm, finer than size of cement, but much coarser than that of silica fume (approximately 0.1 μm), may not have as strong an effect on the reduction of porosity in the interfacial zone in concrete as the silica fume [31]. Figure 2.9 shows SEM image showing the relative interfacial thickness reading pattern.

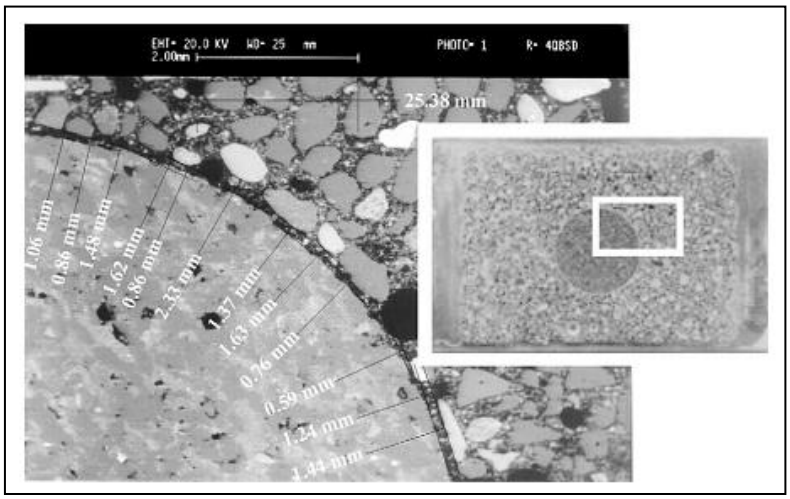

Fig. 2.9 SEM image showing the relative interfacial thickness reading pattern [62].

In previous researches, bond between aggregate and cement paste is an important factor in the strength of concrete, especially the flexural strength, but the nature of bond is not fully understood. Bond is due, in part; to the interlocking of the aggregate and the hydrated cement paste due to the roughness of the surface of the former [62]. It is also revealed that, bond is affected by other physical and chemical properties of aggregate, related to its mineralogical and chemical composition [63].

The effects of the addition of pozzolanic material to the interface of new-to-old paste on the enhancement of bond strength has been found that it can give a significant effect to the bond strength as well as improved the interfacial zone characteristic of concrete. It was suggested that increased effect of the bond strength at interfacial zone depended on the SiO_2 and CaO contents in the additives; higher SiO_2 and/or lower CaO contents were preferred [64]. This study suggests that the structure of the interfacial zone can be modified sufficiently by controlling the chemical components of the additives; even the use of fly ashes consisted of relatively high CaO and low SiO_2.

2.4 Summary and Gap Analysis

After detailed review of the available literature on rice husk ash concrete, it is understood that most of the research was focused on finding a method of burning rice husk to get an optimum properties rice husk ash for partial replacement of cement in concrete.

The literature showed some significant gaps in the area of research on method of burning rice husk ash. Some of conspicuous gaps are obtained as:

a. Method of burning rice husk in producing optimum properties of ash.
b. Characteristic of concrete containing MIRHA comprises of compressive strength, porosity and interfacial transition zone.

Some of the gaps derived from literature review were investigated in this research study.

CHAPTER III
METHODOLOGY

3.1 Test Programme

The quality of concrete is a standard requirement in construction. There are several factors that affect the quality of concrete such as the strength of concrete in compression. This strength is affected by the characteristic of interfacial zone which is divided into macro and micro level. This chapter presents a laboratory works as part of material preparation, sampling and test arrangement.

The absolute volume method adopted in calculation is the mixture proportions. Microwave-incinerated rice husk ash (MIRHA), Sg. Ranggam RHA (SGR-RHA) and Sg. Manik (SGM-RHA) were incorporated as a partial replacement of cement on a weight basis. A number of mixes have been chosen, so that the performance of concrete with different admixtures can be compared. MIRHA, SGR-RHA and SGM-RHA were then used to replace 5%, 10%, 15% and 20% of cement content in concrete with 0.45 w/c.

The control concrete was designated for normal concrete (NC) without any addition of MIRHA, SGR-RHA and SGM-RHA. Superplasticizer was used in concrete containing RHA to enhance workability of concrete. The complete mixture proportion is shown in Table 3.1. The amount of water, fine and coarse aggregates are 213.75 kg/m^3, 607.25 kg/m^3 and 1127.75 kg/m^3 respectively and kept constant throughout the mix proportion.

Table 3.1 Mixture Proportions of Concrete

RHA Replacement		SP	Cement	Water	Fine Aggregate	Coarse Aggregate
(%)	(kg/m³)	(%)	(kg/m³)	(kg/m³)	(kg/m³)	(kg/m³)
0	0.00	0.0	475.00	213.75	607.25	1127.75
5	25.00	0.4	450.00			
10	50.00	0.8	425.00			
15	70.00	1.5	405.00			
20	95.00	2.0	380.00			

Testing of concrete specimens was conducted for fresh and hardened concretes. Beside the tests on concrete specimens, XRD and XRF tests were performed to analyze the properties of raw material. Table 3.2 shows the experiment detail in this research.

Table 3.2 The Experiment Detail for Concrete Specimen Test

Concrete Type	Test Type	Standard	Equipment	Testing Age	Sample Size	Number of Test	Measurement Unit	Type of Measurement
FRESH CONCRETE	Slump Test	BS EN 12350-2:2000	Slump Cone	Fresh Concrete	-	each batch	mm	Workability
HARDENED CONCRETE (Destructive Test)	Compression Strength	BS EN 12390-3:2002	Compression Testing Machine	3, 7, 28, 56 days	150 mm^3 cube	3 cubes / mix/age	N/mm^2	Crushing Strength
	Push-out Test	-	Universal Testing Machine	28 days	30 mm Ø x 30 mm high cored concrete	3 cubes / mix	N/mm^2	ITZ Bonding Strength
HARDENED CONCRETE (Non Destructive Test)	Porosity	ASTM: C 1202	Glass Vacuum Dessicator	28 days	50 mm Ø x 40 mm high cored concrete	3 cylinder / mix	cm^3/s	Void Space
	SEM	ASTM: E3 & E766	LEO 1430 VP Inca X-Sight Oxford Instrument	28 days	10 mm Ø x 2 mm high cored concrete	3 slices / mix	-	Microstructure characteristic

3.2 Sample Preparation

3.2.1 Material

The key ingredients of concrete are cement, coarse and fine aggregates and water. The various type of RHA as a cement replacement in concrete is also elaborated.

3.2.1.1 Rice Husk Ash (RHA)

For the study purpose, three different categories of rice husk ash were prepared from three different sources. MIRHA was obtained from burning process of rice husk which collected from Sg. Ranggam, Perak and was burnt by using UTP microwave incinerator, SGM-RHA collected from conventional rice mill in Sg. Manik, Perak, while SGR-RHA is obtained from modern rice mill in Sg. Ranggam, Perak, Malaysia.

3.2.1.1.1 Sg. Manik Rice Husk Ash (SGM-RHA)

Figure 3.1 shows the Cyclonic Husk Furnace (CHF) used in rice milling plant in Sg. Manik, Perak. The system of burning rice husk used to get the source of the hot air supply to the paddy dryers. The furnace transfers the rice husk from the feed hopper into the combustion chamber, where it was burnt on top of a grate. The spiraling vortex of air forces ash fall to the bottom with special cooling system 35 C temperature of touchable ash reduce no water necessary.

Figure 3.1 Cyclonic Husk Furnace (CHF) & SGM-RHA

The husk was burnt at 1000°C. The ash was then moved to the ash outlet from new husk that was pushed into the combustion chamber. The combustion air enters at the primary air inlet on top of the furnace chamber and was sucked through the burning rice husk bed by the blower of the dryer, which is positioned at the flue gas outlet. The furnace reduces energy costs by the replacing the oil burner and gas fired furnaces.

This husk furnace also complete with auto controlled husk feeder by a variable speed inverter with pid control ensure regular and even hot air supply minimum time delay between start up and actual operation (temperature increase from 0°C to 150°C with in 10 minutes). This method of burning produced SGM-RHA with black color. The ash produced as fertilizer for agriculture sectors.

3.2.1.1.2 Sg. Ranggam Rice Husk Ash (SGR-RHA)

Rice husk at rice mill in Sg. Ranggam, Perak also used rice husk as fuel for boiler to provide steam for production line in rice processing plant. In this burning process, the rice husk was burnt in the range of 600°C to 900°C. Figure 3.2 shows a boiler system in Sg. Ranggam rice milling industry which applied Model KC 8 rice husk/straw gasification system while Figure 3.3 shows the SGR-RHA.

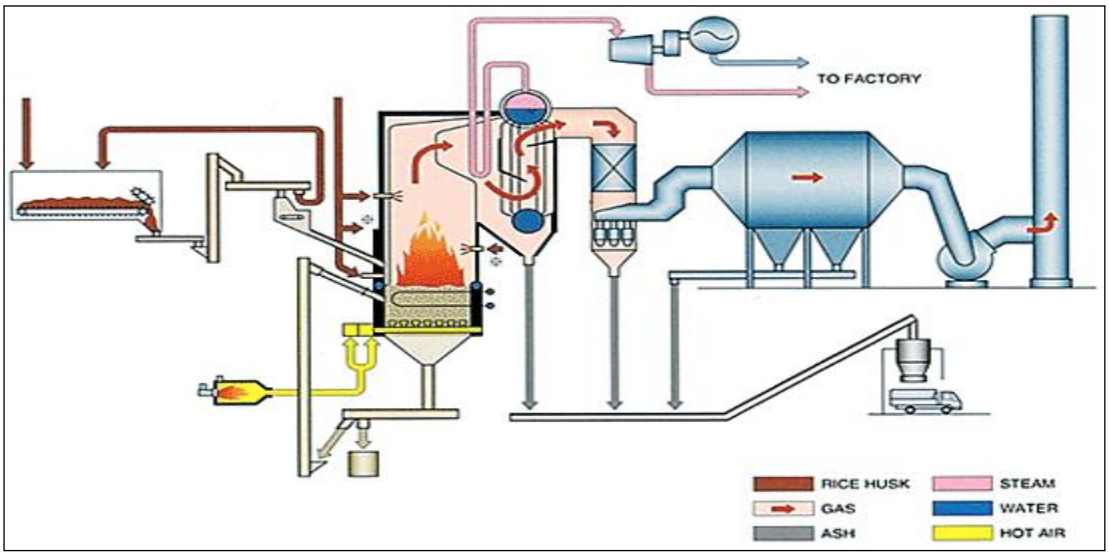

Figure 3.2 Boiler System

Figure 3.3 SGR-RHA

The system was fixed bed, up-draft, sub-stoichiometric, multi-zoned gasification air and staged combustion air. It was available in a wide range of sizes to gasify from 20 - 2,000 tons per day. It includes a fuel metering bin, solids infeed control; multi-zoned gasification air; the KC Reactor®, staged combustion air; combustion chamber; water cooled ash discharge conveyors; utility piping and instrumentation/electronic controls to provide complete automatic or manual operation.

Then, depending on the needs, the syngas produced would be fully combusted for heat applications, partially combusted in a staged configuration for steam applications. This system provided direct heat from rice husk burning for rice factory uses. Referring to the burning process, exhaust from burning rice husk does not contain a lot of CO_2 and dust compared with using burning fossil fuel. This burning process also produces RHA (assigned as SGR-RHA) which possess black dark ash with white spots due to its high burning temperature.

3.2.1.1.3 Microwave Incinerator Rice Husk Ash (MIRHA)

Figure 3.4 illustrates the microwave incinerator used in this study. The UTP Microwave Incinerator (UTPMI) used in the research adopt (or combine) the Air Cooled Magnetron system with an overall dimension of 2.3(H)x4.0(W)x4.0(L) with a chamber capacity of 1 m^3. Ceramic filter is used in the emission and ash control system with PLC mode of operation. Flue Gas Filter that is equipped to the microwave incinerator provides significant positive effect to the environment.

It distils all the dust and ashes from rice husk incineration, hence the air pollution from burning process can be reduced [36]. The temperature range is up to 1600°C with operating temperature of 800°C. Technical specifications of the microwave incinerator are shown in Appendix B.

Figure 3.4 UTP Microwave Incinerator & MIRHA

Rice husks were dried under direct sunlight to reduce their moisture content so that when they were burnt they would not produce large amount of smoke. The microwave incinerator had the temperatures set at 800°C, 700°C and 600°C in order to establish the optimum burning temperature. Tables 3.3 to 3.5 show the burning procedure by using microwave incinerator that was employed in this research. As it can be observed in Figure 3.4, the RHA from microwave burning (MIRHA) have both black and white ash, while RHA from both rice paddy milling were totally in black color.

Table 3.3 Burning Procedure for 800°C Burning Temperature

Phase	Temperature	Duration	Remarks
Phase I	25°C - 150°C	3.5 hours	Remove the carbon and other volatile materials
Phase II	150°C – 800°C	1 hour	Burning Process
Phase III	800°C - 150°C	20 hours	Cooling
Phase IV	150°C - 25°C	1 hour	Cooling in tank until it reached ambient temperature

Table 3.4 Burning Procedure for 700°C Burning Temperature

Phase	Temperature	Duration	Remarks
Phase I	25°C - 150°C	3.5 hours	Remove the carbon and other volatile materials
Phase II	150°C – 700°C	40 minutes	Burning Process
Phase III	700°C - 150°C	19 hours	Cooling
Phase IV	150°C - 25°C	1 hour	Cooling in tank until it reached ambient temperature

Table 3.5 Burning Procedure for 600°C Burning Temperature

Phase	Temperature	Duration	Remarks
Phase I	25°C - 150°C	3.5 hours	Remove the carbon and other volatile materials
Phase II	150°C – 600°C	30 minutes	Burning Process
Phase III	600°C - 150°C	18 hours	Cooling
Phase IV	150°C - 25°C	1 hour	Cooling in tank until it reached ambient temperature

Grinding of MIRHA, SGR-RHA and SGM-RHA are conducted using a Los Angeles abrasion machine with 3000 cycles.

3.2.1.2 Aggregate

The fine aggregate used was natural sand with the fineness modulus 2.7 and classified in Zone 3 while coarse aggregate used was crushed aggregate with the maximum size of 20 mm according to BS 812-103.2 1989 [65]. Sieve analysis of coarse and fine aggregates are shown in Table 3.6 and Table 3.7 whereas gradation curves for coarse and fine aggregate are shown in Figure 3.4 and Figure 3.5 respectively.

Table 3.6 Sieve Analysis Results of Coarse Aggregate

Sieve Size (mm)	Mass Retained (g)	% Mass Retained	Σ % Mass Retained	% Finer
20.00	11	0.50	0.50	99.50
14.00	1078	54.00	54.50	45.50
10.00	682	34.13	88.63	11.37
5.00	224	11.21	99.84	0.16
2.36	1	0.05	99.89	0.11
0	2	0.10	99.99	0.01

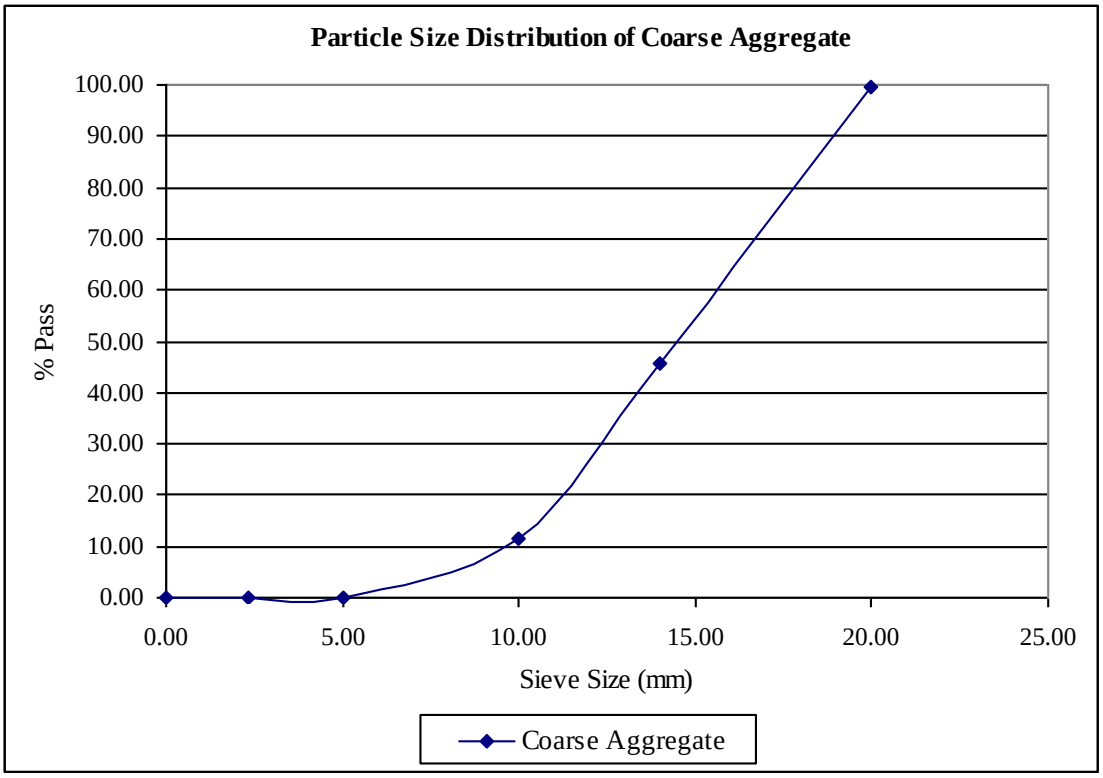

Figure 3.5 Particle Size Distribution Chart of Coarse Aggregate

Table 3.7 Sieve Analysis Results of Fine Aggregate

Sieve Size (mm)	Mass Retained (g)	% Mass Retained	Σ % Mass Retained	% Finer
2.36	74	14.80	14.8	85.20
2.00	20	4.00	18.80	81.20
1.18	86	17.20	36.00	64.00
0.60	127	25.40	61.40	38.60
0.43	84	16.80	78.20	21.80
0.30	74	14.80	93.00	7.00
0.21	22	4.40	97.40	2.60
0.15	8	1.60	99.00	1.00
0.08	4	0.80	99.80	0.20
0.00	1	0.20	100.00	0.00

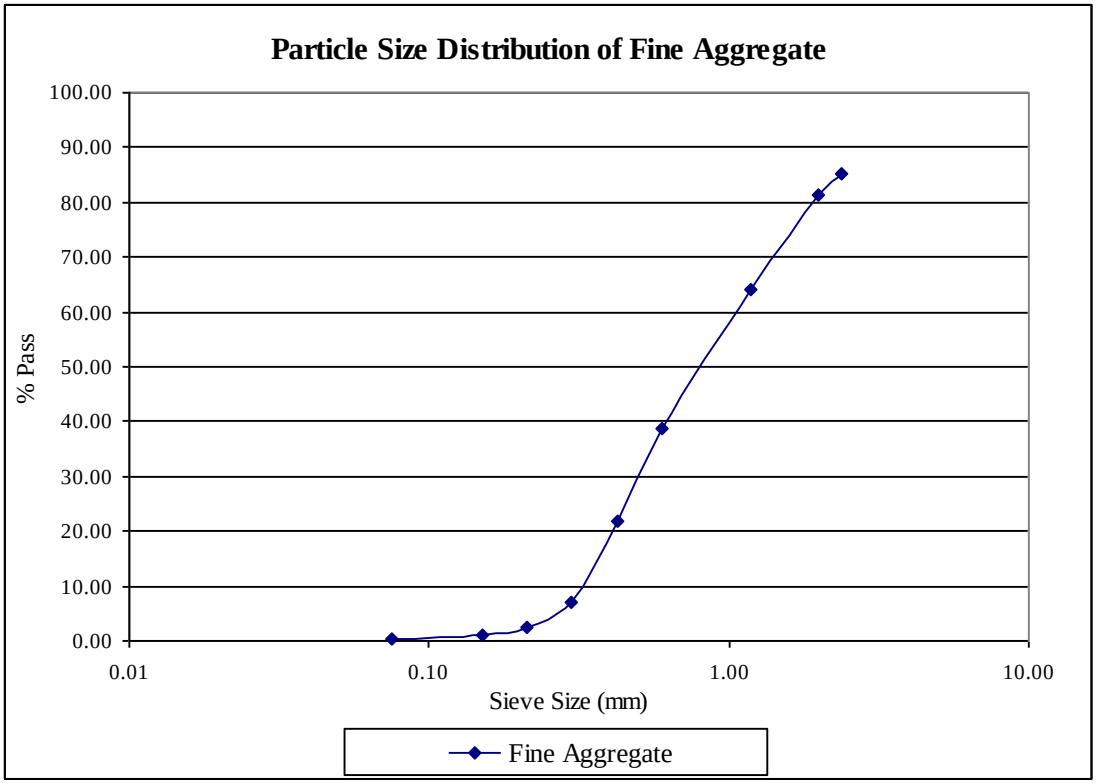

Figure 3.6 Particle Size Distribution Chart of Fine Aggregate

3.2.1.3 Water

Water is an extremely important part of concrete, and drinking quality water is usually required, or water from an approved source free from impurities. The water used in the mix was free from harmful chemicals, oil, cholride, silt, or any harmful ingredients that could impact the performance of the concrete according to BS EN 1008:2002 [66].

3.2.1.4 Cement

Ordinary Portland Cement (OPC) Type 1 was used in this research, according to BS EN 197-1 2000 [67] with the physical and chemical properties listed in Table 3.8. OPC Type 1 was preferred because the observation on concrete properties can be done in normal hydration process hence the advantages of MIRHA usage in concrete can be optimised.

Table 3.8 Physical and Chemical Properties of OPC Type 1 [68]

Modulus	Lime Saturation Factor	0.96
	Silica Modulus	2.37
	Iron Modulus	1.58
Compressive Strength (N/mm^2)	3 Days	38
	7 Days	46
	28 Days	56
Chemical Ingredients (%)	SiO_2	19.98
	Fe_2O_3	3.27
	Al_2O_3	5.17
	CaO	63.17
	MgO	0.79
	SO_3	2.38
	Total Alkalis	0.90
	Insoluble Residue	0.2

3.2.1.5 Superplasticizer

Superplasticizer (SP) used was high range water-reducing concrete admixtures that meet the requirement of BS EN 934-2:2001 [69]. Superplasticizer Sikament-163 was used to maintain a constant workability; expressed as constant slump without any additional amount of mixing water and without any direct effect on the compressive strength of the concrete. It was composed of sodium salt (sulfonated) naphthalene formaldehyde condensate.

3.3 Mixing and Sampling

It is essential that the concrete ingredients are properly mixed according to BS 1881-125.1986 [70] so as to produce fresh concrete in which the surface of all aggregate particles is coated with cement paste and which is homogenous on the macro-scale and therefore possessing uniform properties. Slump test in this research was conducted according to BS EN 12350-2:2000 [71]. It used steel cone mould 305 mm high with small opening at the top. The target slump of all concrete mixed with different percentages of RHA was in the ranged between 30 mm and 60 mm, using suitable doses of superplastizer (SP).

3.3.1 Compressive Strength

The concretes were prepared in the laboratory using a 1.0 m^3 capacity of mixer. Cubes of 150 mm x150 mm x150 mm dimension were prepared for the compressive strength test and compacted using a poker vibrator [72]. After casting, the moulded specimens were covered with plastic sheet and left in the casting room for 24 hours. They were then demoulded and moved into the curing tank with the temperature range between 18°C and 22°C until testing.

3.3.2 Porosity

The concretes were prepared in the laboratory using wooden moulds size of 400 mm x 400 mm x40 mm dimensions and compacted on table vibrator. After casting, the

concrete planks were covered with plastic sheet and left in the casting room for 24 hours. After that all specimens were demoulded and move into the curing tank at room temperature until the desired age of testing. At the defined ages for testing: three 50 mm diameter discs were cored-out from the slab of concrete.

3.3.3 Push-out Test

The test specimens used in the aggregate push-out experiments composed mainly of two parts; the mortar matrix and the cylindrical aggregate. Figure 3.5 shows the aggregate push-out test specimen. The types of mortar used were plain and SGR-RHA, SGM-RHA and MIRHA mortars. The RHA mortar samples adopted 5%, 10%, 15% and 20% of partial replacement of cement content. The cylindrical aggregates were granite with 30 mm diameter.

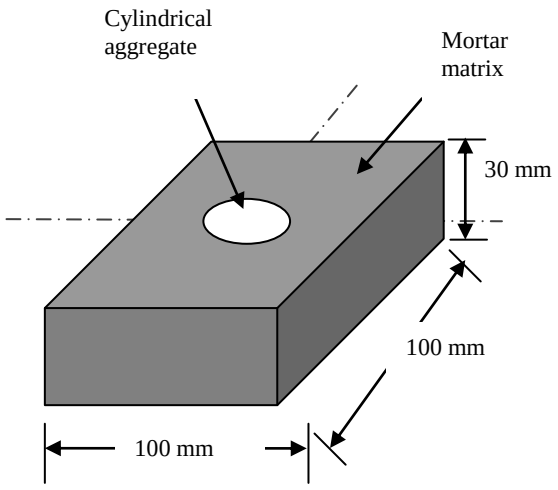

Figure 3.7 Schematic view of a push-out test specimen

The cylindrical aggregates were cored from mother rock sand cut to a length of 30 mm and was placed at the central hole at the bottom of the 100 mm cube steel mould to maintain its precise vertical position during casting. After applying a thin layer of lubricant to the mould and locating the aggregate in the center, the gap between the aggregate and the inner surface of the mould was filled with mortar on a vibrating table.

The moulded specimens were then covered with plastic sheet and left in the casting room for 24 hours. The specimens were then demoulded and moved into the curing tank with the temperature range between 18°C and 22°C. After 28 days the samples were ready to be tested in aggregate push out machine.

3.3.4 Scanning Electron Microscope (SEM)

This test method covers the measurement of metallic coating thickness by examination of a cross section with a scanning electron microscope (SEM). The test specimens for microstructural investigation were cored from concrete cast in a wooden moulds size of 400 mm x 400 mm x 40 mm dimensions. The specimens were cored using coring machine size of 1 inch diameter. For thin section preparation for microstructural investigation, the cylindrical concretes were grind and polish (as showed in Figure 3.6) before the specimens were cut off (1 mm thickness) using diamond cutter showed in Figure 3.7.

Figure 3.8 Grinder & Polisher Machine

Subsequently, in the grind process, Grade 120, 320, 600, 800 and 1200 of paper were used with grinding times of 30 s on each paper; altered the direction of scratches by 90° for each change of paper. Then the specimens were polished successively with 6 and 1-µm diamond paste on microcloth.

Figure 3.9 Diamond Cutter

3.4 TESTING ARRANGEMENT

3.4.1 X-Ray Fluorescence (XRF) Test

Figure 3.8 shows the X-Ray Spectrometer used in this research. X-Ray Fluorescence (XRF) analysis was performed to determine the content of various chemical oxides in RHA samples, SGR-RHA, SGM-RHA and MIRHA. The analysis was carried out using spectrometer of Bruker Axs S4Pioneer referring to BS EN 12677 [40] for the standard of test.

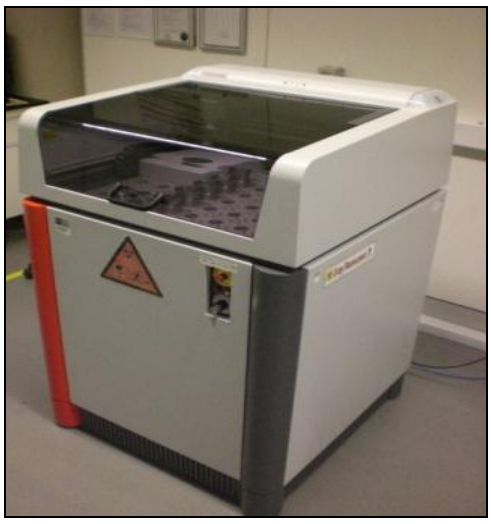

Figure 3.10 Bruker Axs S4 Pioneer X-Ray Spectrometer

All powder samples of RHA were compacted in a specific container using hand compactor before brought into the spectrometer. The analyzed result was captured using the installed software.

3.4.2 X-Ray Diffraction (XRD) Test

X-Ray Diffraction (XRD) analysis was carried out using Diffractometer of Bruker Axs D8 Advance. The purpose was to analyze the crystalline properties of SGR-RHA, SGM-RHA and MIRHA samples and to detect the presence of various crystal system (or molecules) of SiO_2 in each samples. The samples were taken from sieved SGR-RHA, SGM-RHA and MIRHA that will be incorporated into the concrete mixture. A small amount of each powder samples was provided into the X-Ray Diffractometer in a specific container and the analysis results will be displayed using installed software. Afterward, the XRD result will be used to describe the effect of SGR-RHA, SGM-RHA and MIRHA into the concrete properties during maturing period. Figure 3.9 shows the X-Ray Diffractometer used in this research. This test was conducted according to ASTM D3906-03 [73].

Figure 3.11 Bruker Axs D8 Advance X-Ray Diffractometer

3.4.3 Compressive Strength Test

Compressive strength development of the concrete sample was measured according to BS EN 12390-3:2002 [74] using Digital Compressive Testing Machine as referred to in Figure 3.10. Since destructive testing method is directly considered, compressive strength test was done after which non destructive tests were completed. The measurement was taken for three concrete cubes per mix at ages 3, 7, 28, and 56 days. During the test, concrete cube was loaded with constant loads without any sudden shock loads. Compressive strength value was then taken from ultimate load that can be sustained by the concrete cube divided by surface area of the cube.

Figure 3.12 Digital Compressive Testing Machine

3.4.4 Porosity

Total porosity of samples was determined according to the vacuum saturation method that was developed by RILEM [75] using the Equation 1 stated below:

$$P = \frac{W_{sat} - W_{oven}}{W_{sat} - W_{water}} \times 100 \qquad (1)$$

Where, P is the total porosity in percentage, W_{sat} is the weight of saturated samples measured in the air; W_{oven} is the weight of oven dried samples measured in the air, and W_{water} is the weight of saturated samples measured in water, all weight measurement are in g. Figure 3.13 shows a glass vacumn Dessicator which is used in this study.

Figure 3.13 Glass Vacuum Dessicator.

3.4.5 Push-out Test

Many researchers have used different techniques and test methods to study the interfacial bond as there is no universally accepted and standardized test method. This has led the researchers [76-79] to utilize the test samples, which contain an artificially prepared (mostly cored) single aggregate. This allows one to apply the load directly to the aggregate, and to locate the aggregate in any desired location within the concrete body [62].

The interfacial bond strength was tested at 28 days of curing. For each percentage of inclusion of each RHA samples, three specimens were tested, which makes 21 test specimens in total. Aggregate push-out tests were conducted using the general set-up

shown in Figure 3.14. The load was applied only to the cylindrical aggregate portion of the specimen, while the mortar matrix was fully supported except for a 0.5 mm rim around the cylindrical aggregate to allow the aggregate to be pushed through the circular hole without any disturbance. Interfacial bond strength, τ (N/mm^2) was obtained by dividing the maximum load, P_{max} by the nominal shear area which is given by the product of the circumference of the cylindrical aggregate and the depth as Equation 2 shown below:

$$\tau = \frac{P_{max}}{2\pi rL} \qquad (2)$$

Where L is the constant length of the cylindrical aggregate (30 mm) and r is the radius in mm (30 mm).

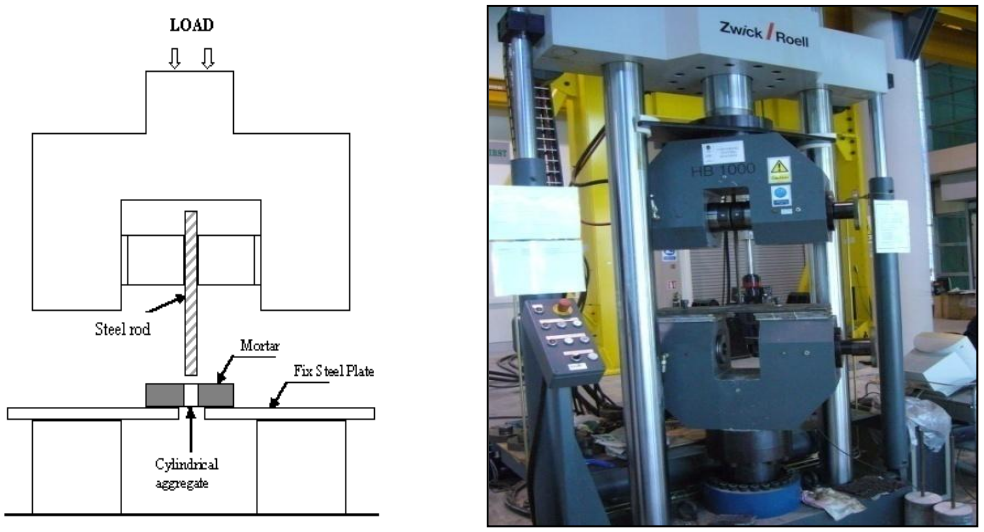

Figure 3.14 Schematic Diagram and Aggregate Push-Out Test Apparatus.

3.4.6 Scanning Electron Microscope (SEM)

Scanning Electron Microscopy (SEM) analysis was carried out to describe the inner condition of concrete samples with and without replacement of SGR-RHA, SGM-RHA and MIRHA.

Each sample was cured for 28 days and then dried up in ambient temperature for 48 hours until the water evaporated from concrete pores. The analysis was performed with LEO 1430 VP Inca X-Sight Oxford Instrument. This type of SEM needs the sample to be conductive for full observation. Concrete as a non-conductive material must be coated with gold atoms in sputter coater. Coated concrete was then placed in the vacuum chamber inside the SEM. The SEM must be operated in specific pressure to facilitate the operation of filament and electron inside SEM [80]. Figure 3.15 shows the SEM used in this research.

Figure 3.15 LEO 1430 VP Inca X-Sight Oxford SEM Instrument with Sputter Coater.

CHAPTER IV
RESULTS AND DISCUSSIONS

4.1 Introduction

In the previous chapter, the methods and materials required to prepare and produce good quality concrete model were discussed. The proposed burning temperatures and various percentage of inclusion of RHA were used to understand the behavior of concrete. This chapter presents and discusses the results of laboratory work.

4.2 Chemical Compositions of Materials

X-Ray Fluorescence (XRF) analysis is proficient in analyzing material contents inside SGR-RHA, SGM-RHA and MIRHA, hence the amount of SiO_2 can be observed. The presence of various materials within all samples as can be seen in Table 4.1.

Table 4.1 Chemical composition of OPC, MIRHA, SGR-RHA and SGM-RHA

Oxide	Weight %					
	OPC	MIRHA 800	MIRHA 700	MIRHA 600	SGR-RHA (600°C-900°C)	SGM-RHA (1000°C)
Na_2O	0.0164	0.1215	0.0725	0.0195	0.0203	0.0371
MgO	1.4334	0.4864	0.5036	0.5885	0.3562	0.5696
Al_2O_3	2.8357	0.4473	0.4181	0.3572	0.4889	0.9607
SiO_2	20.444	89.3430	87.2145	86.3115	90.3289	90.3615
P_2O_5	0.1023	2.5792	3.0006	3.008	2.5118	2.3052
K_2O	0.2646	4.9756	6.1856	6.3366	4.5351	4.2964
CaO	67.734	0.7584	0.8106	0.9996	0.5634	0.8627
TiO_2	0.1701	0.0183	0.0184	0.0191	0.0843	0.0278
Fe_2O_3	4.6352	0.3971	0.3957	0.7227	0.3900	0.2907
SO_3	2.2020	0.8952	1.3131	1.5145	0.6458	0.2038
MnO	0.1614	0.0807	0.0836	0.1301	0.0667	0.0844

It is evident that burning RHA with higher temperature will give higher silica content. Despite of no significant difference of SiO_2 content between all samples but MIRHA burnt at 800°C showed a highest of SiO_2 quantity. It is shown that among sample of MIRHA, sample burnt at 600°C shows the lowest percentage of SiO_2. MIRHA 600 is 3.39% lower than MIRHA 800 meanwhile MIRHA 700 shows 2.38% lower than MIRHA 800. It is believed that different burning temperature could give the significant effect to the ash produced: the higher the burning temperature the higher quantity of SiO_2 can be obtained. This has been confirmed by two other samples of SGR-RHA and SGM-RHA. The higher SiO_2 produced as burning temperature increased. It is noted that SGR-RHA shows 1.10% higher than MIRHA 800 meanwhile SGM-RHA exhibits 1.14% higher than MIRHA 800 samples. When it observed on SiO_2 quantity of samples SGR-RHA and SGM-RHA, it is found that there is not much different on percentage due to the burning temperatures which in the same range 900°C-1000°C.

From the result also, among MIRHA samples it noticed that percentage of Na_2O decrease with the decrease of burning temperature and at the same time, the percentage of K_2O increase as burning temperature increase. This may be probably due to the different burning temperature and burning method. Referring to the composition of Na_2O, it is noted that with different burning method, high burning temperature cannot assured the decreasing of Na_2O. A SGR-RHA sample shows it contains only 0.02% of Na_2O and as well as SGM-RHA sample contains 0.04% of Na_2O compared to MIRHA 800 sample which shows a highest percentage 0.12% of Na_2O. And that may also be because the different burning condition compared to burning husk using incinerator. The characteristic of RHA was not only determined using XRF test, but also had been analyzed using X-Ray Diffraction (XRD) test.

4.3 X-Ray Diffraction (XRD)

X-Ray Diffraction (XRD) has been used to analyze the crystalline properties of material. Graph patterns of XRD analysis can show whether the material is in amorphous, partially crystalline, or crystalline state. Graph peaks, which appeared at

2θ scale of 22° and 36°, indicated the presence of SiO_2 cristobalite inside RHA samples. The gradual dense scatter of XRD graph is used to indicate the amorphous state of a material meanwhile the intensity is the degree or level of crystallinity of sample. Nevertheless, although XRD graph shows a sharp intensity of dense scatter, samples could not be categorized as an amorphous or fully crystalline sample. The fully amorphous material is indicated with a smooth gradual scatter, while the fully crystalline material is indicated with a flat and sharp peak of graph scatter.

Figure 4.1 shows a graph of MIRHA sample at 800°C that reveals that the XRD graph has one sharp peak, which indicates that the MIRHA has transformed into a crystalline state. The graph shows that MIRHA's sample transformed into crystal at temperature 800°C due to its long burning process of almost one hour. Previous researches have confirmed that burning RHA with the higher temperature for approximately for 1 hour would lead to a crystalline form of RHA [31, 37].

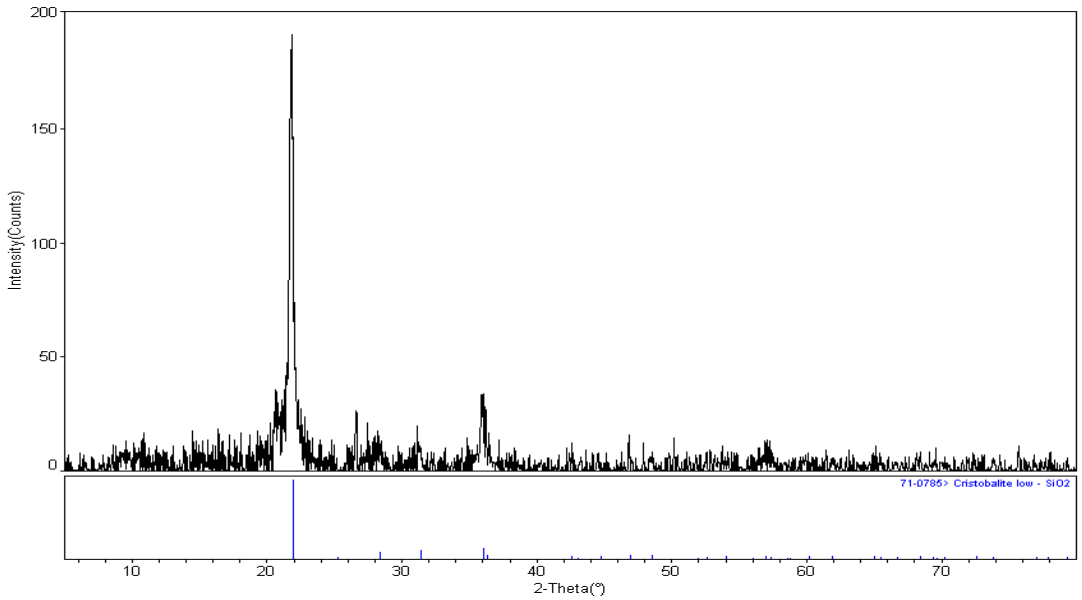

Figure 4.1 XRD Graph of MIRHA Burnt at 800°C – 185 of intensity

Figures 4.2 and 4.3 describe the properties of MIRHA that was burnt at 700°C and 600°C respectively. It shows that the decrease burning temperature will lower the intensity of crystallinity of RHA. Furthermore, it could be noticed that, MIRHA that

was obtained from 700°C and 600°C combustions had low crystalinity according to the XRD intensity. It is observed that, even MIRHA 700°C and MIRHA 600°C had low intensity of crytalinity and medium amorphousness whilst MIRHA 800°C depicts the highest performance on concrete properties.

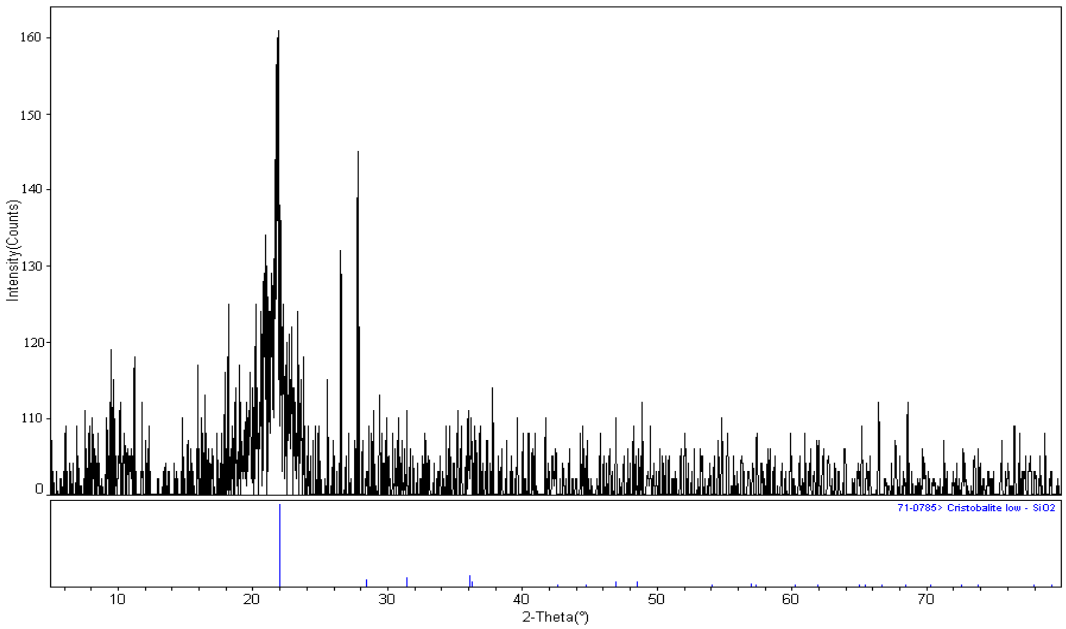

Figure 4.2 XRD Graph of MIRHA Burnt at 700°C – 161of intensity

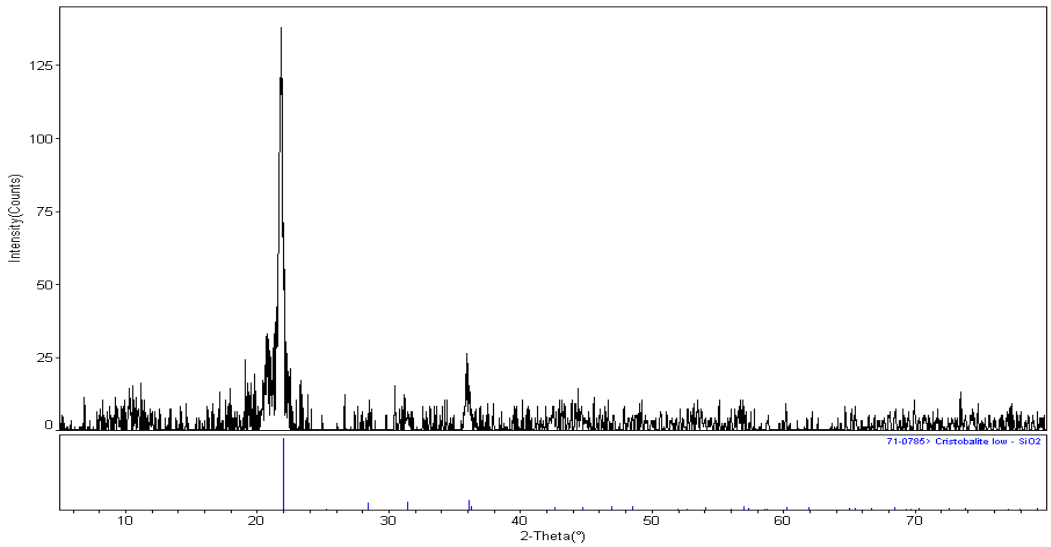

Figure 4.3 XRD Graph of MIRHA Burnt at 600°C – 138 of intensity

Nevertheless, the RHA obtained from rice mills burnt using furnace and boiler proved that even they were burnt within short period of time and cooled down directly in open area; the results as shown in Figure 4.4 and Figure 4.5 reveal that the crystallization still occurred. It is believed that the temperature of burning is the vital element to be controlled. However, the level of amorphousness of RHA samples cannot be determined by a number because the degree of amorphous phase is indicated by a blunt peak of graph.

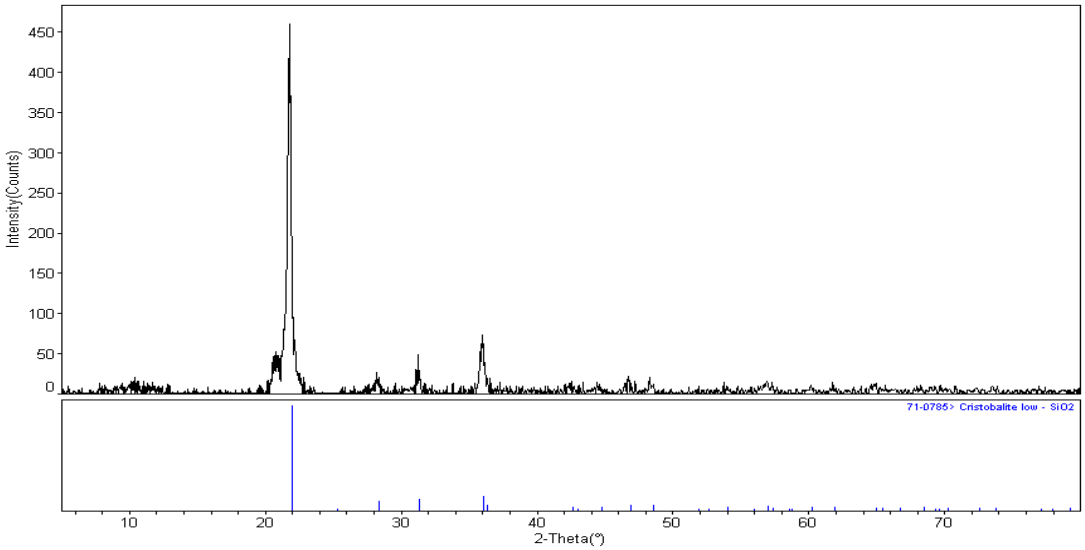

Figure 4.4 XRD Graph of SGM-RHA – 461 of intensity

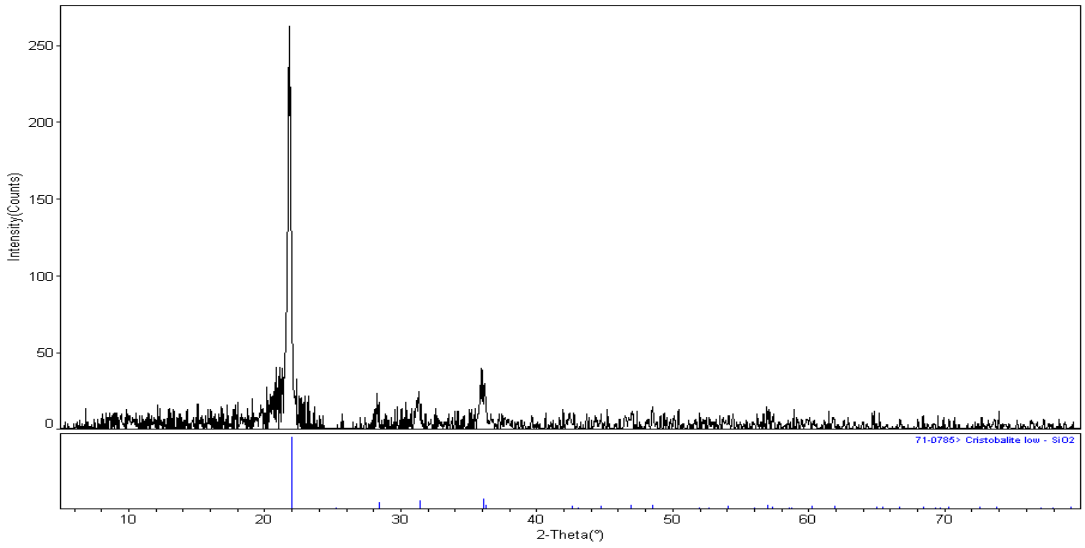

Figure 4.5 XRD Graph of SGR-RHA – 263 of intensity

On the other hand, XRD graphs in Figures 4.1 to 4.5 showed the type of crystalline and level of intensity of RHA. Table 4.2 shows the summary of the effect of burning conditions on the crystal structure for the sample in this research.

Table 4.2 Effect of Burning Conditions on the Crystal Structure

Type	Intensity	Crystalline	amorphousness
OPC	160	Hatrurite	-
MIRHA 800	185	Crystobalite Medium	Medium
MIRHA 700	161	Crystobalite Medium	Medium
MIRHA 600	138	Crystobalite Low	Medium
SGR-RHA	263	Crystobalite High	Low
SGM-RHA	461	Crystobalite High	Low

Based on XRF result, it was observed that low burning temperature produced low SiO_2 content in RHA, while burning rice husk with high temperature presented high SiO_2 content in RHA, but this high temperature would lead to a crystalline state of RHA. It can be seen in the Table 4.2, SGR-RHA and SGM-RHA depict the highest intensity compared to MIRHA samples. It is observed in the samples of RHA the presence of sharp peaks, referring to the cristoballite and the quartz, indicating that a considerable amount of silica did not become silicate. The results showed a distinct peak corresponding to crystalline silica. The reason for this behavior is the long duration of combustion process and the high temperature of burning. It is believed that MIRHA 600 and MIRHA 700 showed the lower result of intensity. It is due to char contain in MIRHA 700 and MIRHA 600. It is believed that, with these two different burning temperatures, not all rice husks were burned instantly, some of them were burnt later. As a result, the husk was not totally burnt and the ash that had been produced with these temperatures was in black ash.

4.4 Compressive Strength

Compressive strength test was conducted to analyze the impact of SGR-RHA, SGM-RHA and MIRHA addition into the concrete mix proportion. The strength development of the concrete samples was measured at 3, 7, 28, and 56 days of age. The data analysis was made for each concrete samples and compared to control concrete (without RHA) and concrete samples containing various percentages of SG-RHA, SGM-RHA and MIRHA. Table 4.3 shows the compressive strength development of all concrete samples.

Table 4.3 Compressive Strength Development of Concrete Samples

Types of RHA	RHA Replacement (%)	Compressive Strength (MPa)			
		3 days	7 days	28 days	56 days
Normal Concrete	0	21	26	39	50
MIRHA 800	5	44	52	61	72
	10	41	50	59	66
	15	33.3	41.6	49	57.9
	20	25	37.8	55	63
MIRHA 700	5	26.1	40.9	57	65
	10	33.3	44.6	59	68
	15	29.2	42.1	55	60.3
	20	27.7	41.4	49.7	55
MIRHA 600	5	38	44.5	58	65
	10	31.7	41.2	49.5	59
	15	29.2	42.1	55	60.3
	20	27.7	35.3	42.5	57
SGR-RHA	5	30	39	50	60
	10	25	33	48	55
	15	23	31	45	53
	20	19	28	41	51
SGM-RHA	5	29	37	48	56
	10	27	35	46	54
	15	23	31	44	53
	20	19	28	41	51

Addition of all samples of RHA into concrete mixture significantly enhanced concrete strength performance. Compressive strength data of MIRHA at 800ºC concrete were higher than those of the normal concrete, irrespective of age.

4.4.1 Compressive Strength of Concrete Samples of MIRHA 800

Compressive strength data of MIRHA at 800ºC concrete were higher than those of the normal concrete, irrespective of age as shown in Figure 4.6. Higher compressive strength of MIRHA concrete samples compared to control concrete from early curing days also indicated that pozzolanic reaction started to occur even at early ages.

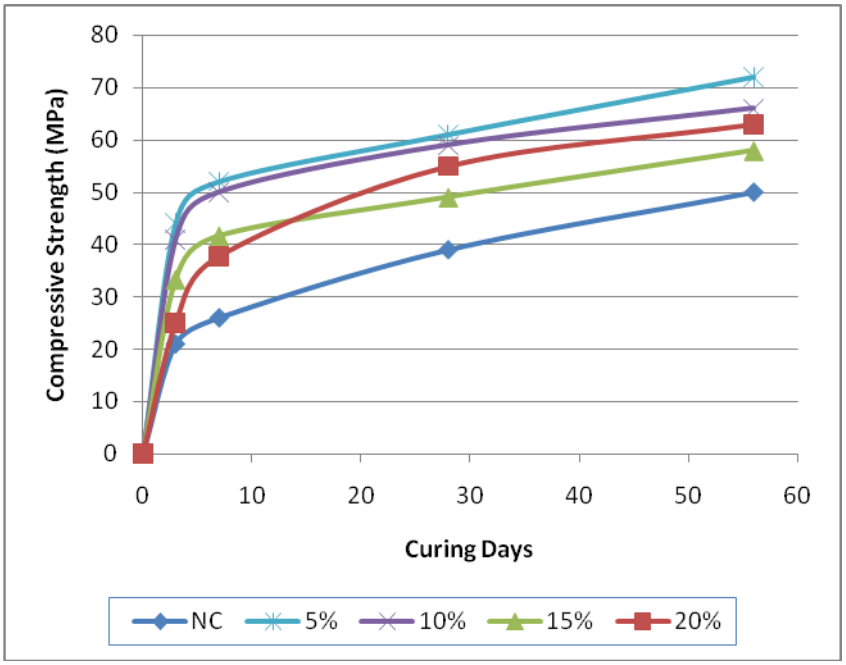

Figure 4.6 Compressive Strength Development of Concrete Sample with MIRHA at 800°C

The development of concrete strength for different percentage inclusion of MIRHA in concrete is shown in the Figure 4.6 and it is observed that the increase percentage of MIRHA directly slow down the compressive strength development of concrete. From early curing days, MIRHA concrete samples have gained strength faster than controlled samples and 5% additions of MIRHA has the highest level of compressive strength among MIRHA at 800°C concrete samples. After 28 days, the

5% MIRHA concrete achieved compressive strength performance 33.33% higher than control concrete, 23.33% higher than 15% MIRHA concrete, and 13.33% higher than 10% MIRHA concrete. There is no significant difference of compressive strength between 5% and 20% MIRHA concrete at 28 days. However, within the short period of 3 and 7 days, the effect of absorptive characteristic of MIRHA that caused lack of water in 20% MIRHA concrete slow down the development of strength. It is believed that the adequate amount of water and high pozzolanic reactivity were the reasons why 5% MIRHA concrete has faster strength acceleration until achieved 56 days.

4.4.2 Compressive Strength of Concrete Samples of MIRHA 700

Figure 4.7 shows the compressive strength development of concrete with MIRHA at 700°C. Result displays that compressive strength developments of MIRHA concrete are significantly higher compared to control concrete.

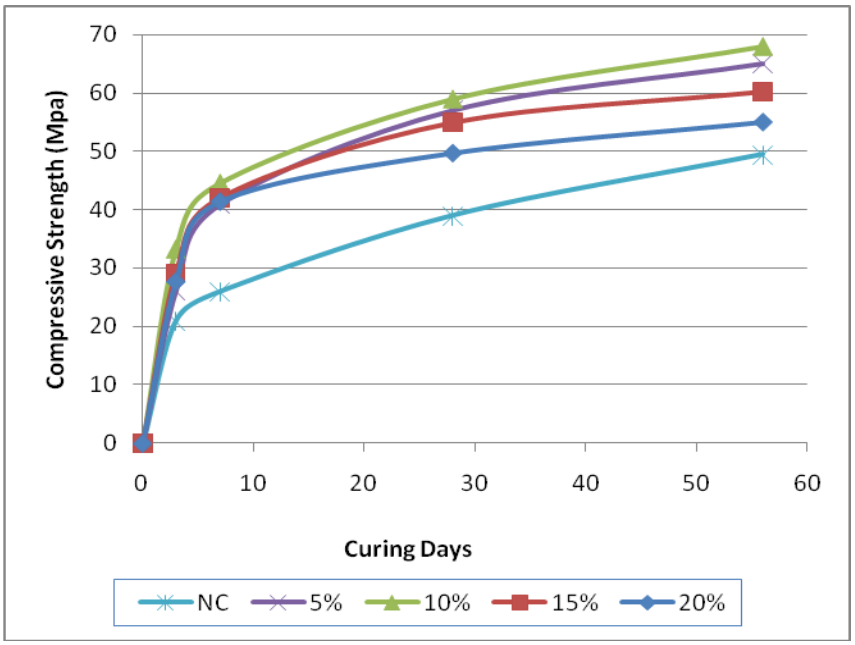

Figure 4.7 Compressive Strength Development of Concrete Sample with MIRHA at 700°C

All MIRHA concrete samples namely 20%, 15%, 10% and 5% replacement of OPC had slightly different strength development at early days. Strikingly, results of up to 28 days show that 10% MIRHA achieved 3.4% higher than 5% MIRHA

concrete and 6.8% higher than 15% MIRHA and 15.3% compared to 20% MIRHA. The reduction of Portland cement replaced by MIRHA that slowed down the hydration process was the main reason of lower strength for 20%, 15% and 5% MIRHA concrete at early days. As the curing continued, pozzolanic reaction in 10% MIRHA concrete showed more rapid development in producing C-S-H gel as indicated by the increment percentage of compressive strength, which indicate that 10% is the optimum level of replacement. Thus, it could be noticed that at 56 days the concrete had a better performance.

4.4.3 Compressive Strength of Concrete Samples of MIRHA 600

Figure 4.8 shows that the higher percentage of MIRHA at 600°C added into the concrete directly, slower down the development of compressive strength. This is due to the declining of Portland cement content in the mix proportion. Eventually, that condition will reduce the production of (C-S-H) gels. The reduction of these gels makes failed to fill up the pores structure inside the concrete and created water-filled space that affect the compressive strength of the concrete.

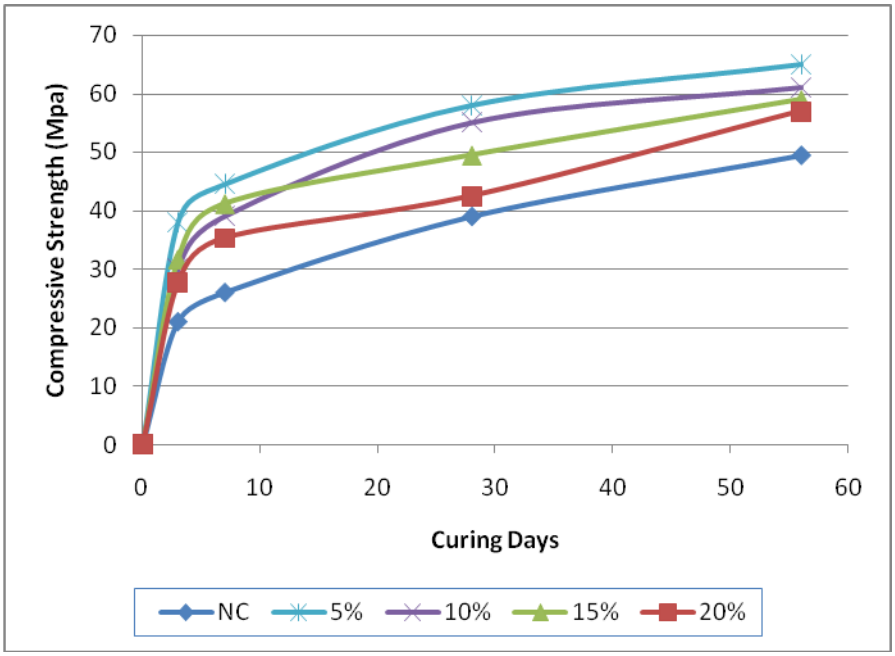

Figure 4.8 Compressive Strength Development of Concrete Sample with MIRHA at 600°C

Lower content of $Ca(OH)_2$ produced also affected the pozzolanic reaction with SiO_2 [81]. Therefore at 20% and 15% MIRHA concrete, strength development was slower since there were larger amount of water-filled spaces left and fewer amounts of C-S-H gels produced. Compared to normal concrete, 20% MIRHA had 7.14% higher strength from normal concrete, meanwhile 15% MIRHA had 16% higher than normal concrete. There is no significant difference in compressive strength between 5% and 10% MIRHA concrete at 28 days but in the early age, 5% MIRHA concrete gained higher compressive strength than 10% MIRHA concrete. Normally, pozzolanic concrete has lower strength than normal OPC concrete at early days, however MIRHA is not following the normal pozzolanic attribute as it is more like silica fume where the addition of silica fume has significant influence on the early strength development of mortar [81]**.** When silica fume is incorporated, the rate of cement hydration increases at the early hours due to the release of OH^- ions and alkalis into the pore fluid. The increased rate of hydration may be attributable to the ability of MIRHA to provide nucleating sites to precipitating hydration products like lime, CSH, and ettringite. With correct mix proportion, MIRHA concrete can achieve early strength higher than normal concrete.

4.4.4 Compressive Strength of Concrete Samples of SGR-RHA

Figure 4.9 illustrates that the replacement of SGR-RHA into the concrete mixture gave slightly similar effects of concrete strength with the concrete contained MIRHA. As it can be observed at fresh state, similar water/cement, SGR-RHA would produce wet concrete without water reducing admixture or superplasticizer added. It is believed that this was mainly due to the size particle of SGR-RHA, affected from high burning temperature that directly increased the surface area. Thus, concrete containing SGR-RHA as well as SGM-RHA produced concrete with high consistency. However, for concrete with high consistency, addition of SGR-RHA and SGM-RHA for high water/cement could decrease the concrete stability and in contrary increase workability, so that allow the tendency towards bleeding and segregation.

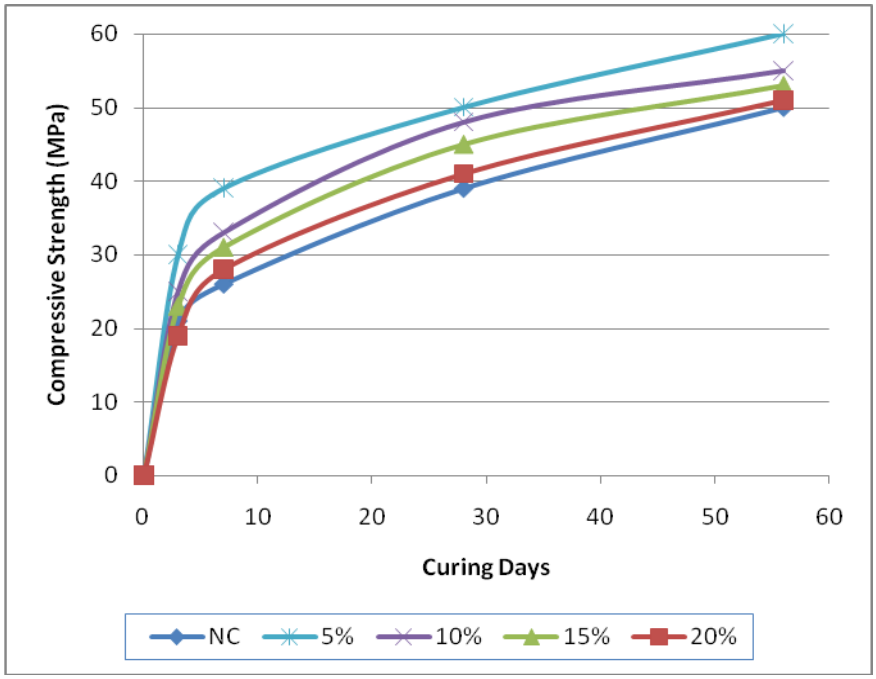

Figure 4.9 Compressive Strength Development of Normal Concrete and Concrete with SGR-RHA

From the figure, it could be noticed that at early days of curing, the addition of SGR-RHA will directly improved the strength of concrete and SGR-RHA-5% shows the optimum replacement. It is not much different of compressive strength at early days within all the percentage of replacement but interestingly, at 56 days the graph shows only 5% replacement gained higher development compared to other percentage. Meanwhile 10%, 15% and 20% replacement had slow development and similarly with normal concrete. Nevertheless, there is no different with SGM-RHA which it could be observed from Figure 4.10.

4.4.5 Compressive Strength of Concrete Samples of SGM-RHA

Figure 4.10 also depicts the optimum of replacement at only 5% of SGM-RHA and in the meanwhile the increase percentage of SGM-RHA added into the concrete directly lowered the performance of concrete. Clearly observed that the increase percentage of SGM-RHA as well as SGR-RHA had made the mixture become more wet and tends to bleeding and segregation. Thus, the hydration process could not perform very well

and had made the concrete less performance compared to 5% of replacement. However, without consideration of percentage replacement, SGR-RHA and SGM-RHA concrete could give a better performance compared to normal concrete. It is believed that the content of SiO_2 and the amorphous of RHA could give a significant contribution to hydration process.

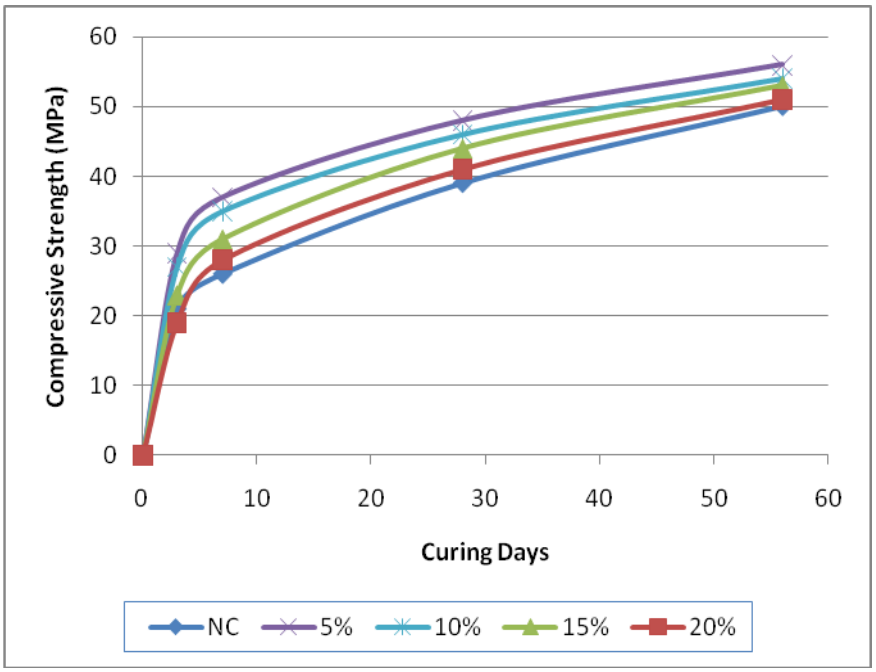

Figure 4.10 Compressive Strength Development of Normal Concrete and Concrete with SGM-RHA

4.4.6 Compressive Strength of Concrete Samples of All Samples

Figure 4.11, shows the comparison of compressive strength development between concrete with MIRHA at 800°C with optimum percentage (5%), concrete with MIRHA at 700°C with optimum percentage (10%), concrete with MIRHA at 600°C with optimum percentage (5%), concrete with SGR-RHA with optimum percentage (5%) and concrete with SGM-RHA with optimum percentage (5%).

It can be concluded that MIRHA-800 had the optimum replacement at 5% provides better acceleration in compressive strength development compared to the MIRHA-700 with 10% replacement and MIRHA-600 with 5% replacement. Referring

to the figure, all specimens was found to had a better performance compared to normal concrete regardless of percentage replacement.

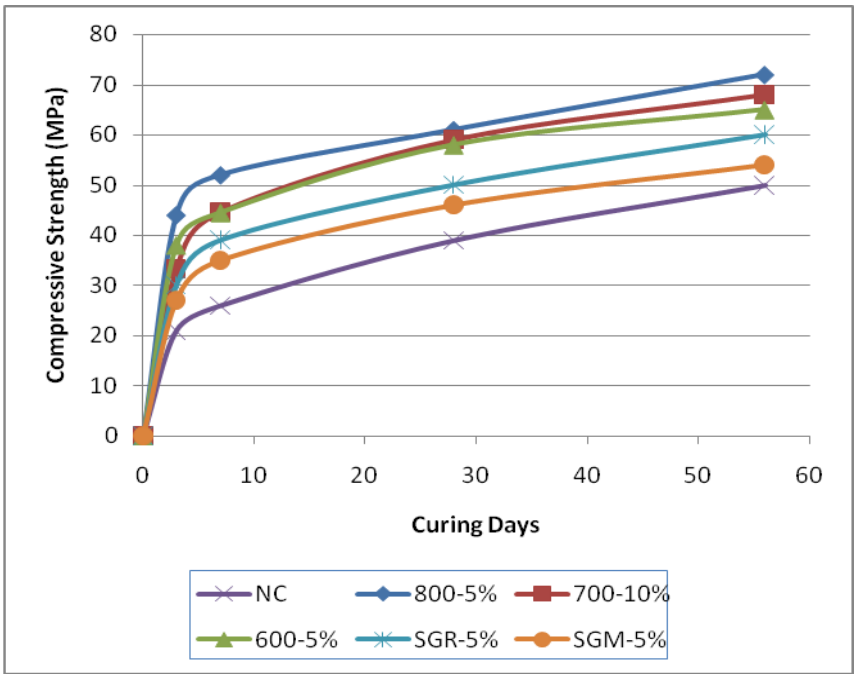

Figure 4.11 Compressive Strength Development of All Concrete Samples

Despite the fact that the SGR-RHA and SGM-RHA had a high intensity of crystallinity, the specimens also showed a good contribution to the performance of concrete compared to normal concrete. However, it can be seen that MIRHA-800 with 5% replacement concrete had superior compressive strength among the other samples, meanwhile among RHA from mills, SGR-RHA concrete samples with 5% replacement performed better compressive strength performance. Perfect amount of water, cement and RHA to react in MIRHA-800 with 5% replacement sample had made the concrete accelerated faster and gained higher strength among the other sample and even on the MIRHA concrete samples.

On the other hand, based on the comparison made between MIRHA concrete and RHA burnt using different method, the strength of MIRHA concrete depicts the highest increment 28 days. Table 4.4 shows the result on strength of concrete with different burning method.

Table 4.4 Comparison of Compressive Strength Development of Concrete Samples

Researcher	Method of Burning	Percentage of replacement (%)	Properties		Production
			Silica (SiO_2) %	Strength Increment at 28 days*	Burning Time
Kartini et. al (2008) [11]	Ferrocement Furnace	20 & 30	94.41	6%	1 day
Kamal et. al (2008) [49]	Microwave incinerator	5, 10, &15	89.34	26-56%	1 day
Nuruddin et. al (2007) [82]	Microwave incinerator	5, 10 & 15	88	27.73%	2 days
Fadzil et. al (2008) [83]	Industrial Furnace	10	83	8.77%	1 day

From the table, it can be seen that strength of concrete contains MIRHA shows the highest increment at 28 days. It is clear that burning RHA using microwave incinerator can absolutely give a better performance of compressive strength. It is due to the optimum silica content and the intensity of crystalinity.

4.5 Porosity

The addition of RHA into concrete mixture significantly enhanced concrete strength performance regardless of burning temperatures and combustion method but increase percentage of RHA added led to higher porosity. It is believed that the process of hydration did not occur completely due to the lack of $Ca(OH)_2$ amount produced by cement. With insufficient amount of $Ca(OH)_2$, pozzolanic reaction could not occur properly and resulted in lower calcium silicate hydrate (C-S-H) gels being produced. Hence, the inadequate amount of water had made MIRHA concrete could not perform pozzolanic reaction effectively due to the absorptive character of RHA and interrupted the cement hydration process to produce $Ca(OH)_2$. Figure 4.12 presented the concrete porosity characteristic of concrete with different binder types.

Concrete pores and water-filled spaces that were expected to be filled with C-S-H gels existed in large number. The ineffective hydration process also had an effect on the irregular pores distribution. The porosity of concrete containing MIRHA was found to be lower than normal concrete regardless of different burning temperatures and percentages inclusion of MIRHA.

According to the Figure 4.12, it can be seen that, the increase percentage of MIRHA replaced into the concrete directly increased the porosity of concrete regardless of burning temperature.

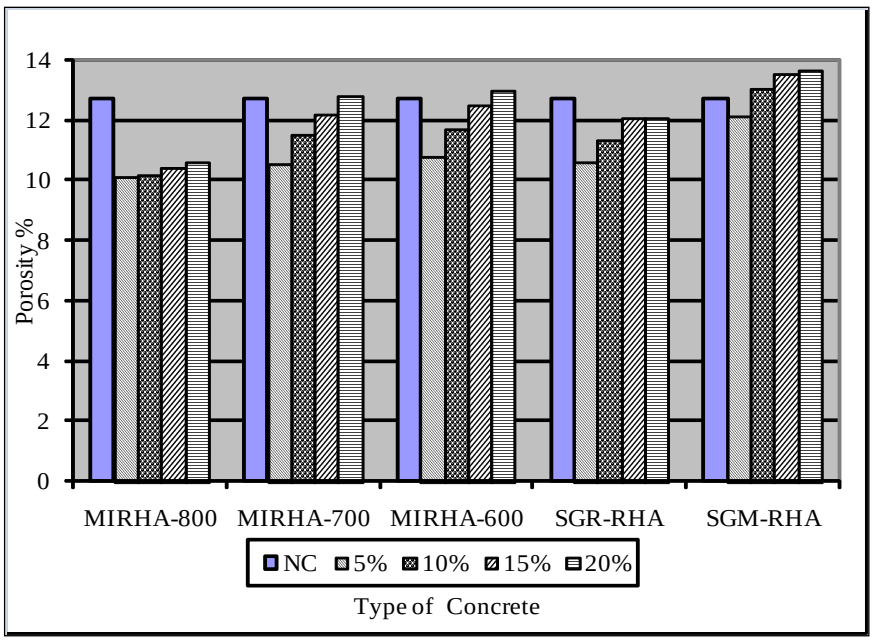

Figure 4.12 Porosity of Normal Concrete and Concrete with MIRHA, SGR-RHA and SGM-RHA

This has been confirmed by two other samples of RHA which are SGR-RHA and SGM-RHA, as same pattern as MIRHA samples were showed in the figure From the figure, MIRHA 800 shows the lowest porosity among other samples. MIRHA 800 with 5% replacement shows 21.28% of reducing the porosity of sample compared to normal concrete, meanwhile MIRHA 700 with 5% replacement shows 17.76% of reducing the porosity of sample compared to normal concrete. SGR-RHA also shows a good reduction on the percentage of porosity at 17.07% but for SGM-RHA samples, it revealed that the ash contributed lesser than other samples which just at 5.27%.

This could be due to the un-hydrated MIRHA, SGR-RHA and SGM-RHA that absorb more water. Nonetheless, the SGM-RHA concretes show that only 5% of inclusion gave a better performance compared to normal concrete while 10%, 15% and 20% inclusion of SGM-RHA lead to increase of porosity. It shows that addition of MIRHA which is more than 5%, to the concrete mixture absorbed water in large amount and cause the mixture to be dry. As shown in the figure, there is only slight difference in porosity between all percentages of MIRHA 800 in concrete. This shows consistency in the amorphousness and highest amount of SiO_2.

It maybe recalled that, even the amount of the SiO_2 increased with the increased of RHA replacement, but other minor compounds also must take into consideration. Referring to XRF result in previous chapter, the present of K_2O is believed has significant contribution on the porosity characteristic. It can be concluded that MIRHA 800 has the optimum chemical composition which can give a great performance compared to normal concrete. In addition, it can be said that with insufficient amount of $Ca(OH)_2$ also, pozzolanic reaction could not occur properly and resulted in lower calcium silicate hydrate (C-S-H) gels being produced. While the first provides a denser interface by acting as a filler and providing secondary hydration products, the second helps towards deflocculation of the cement and MIRHA particles, and reduction in the water content of the mix as well as providing extra consistency. It has been revealed that with correct mix proportion, MIRHA concrete can achieve lower porosity compared to normal concrete.

4.6 Push-Out Test

The purpose of investigating the bonding strength between aggregate and cement paste is to provide evidence of densification by RHA replacement. The result of push-out test and scanning electron microscopy (SEM) are then combined to address the effectiveness of the interfacial transition zone densification on interface bond strength.

4.6.1 Interfacial Bonding Strength of Aggregate/Mortar with MIRHA 800

Figures 4.13 shows the bond strengths of the various mix proportions that incorporated MIRHA burnt at 800°C. From the results, the interfacial bond strengths of all MIRHA pastes were significantly higher compared to plain cement mortar. The 5% inclusion of MIRHA burnt at 800°C in mortar paste shows the highest interfacial bond strength amongst the samples tested.

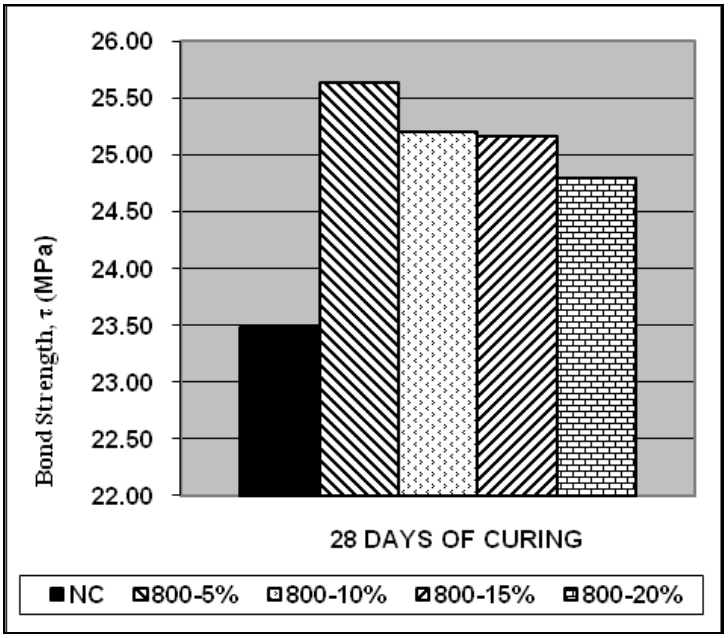

Figure 4.13 Interfacial Bond Strength of Aggregate/Mortar with MIRHA 800

Compared to plain cement mortar, 5% MIRHA paste had 8.41% higher strength than plain cement mortar. There is no significant different of interfacial bond strength between 10% and 15% MIRHA paste. Meanwhile 20% MIRHA paste had lowest interfacial bond strength amongst the MIRHA mortar. It is believed that the effect of absorptive character of MIRHA that caused lack of water in 20% MIRHA paste and slower the development of strength. It can therefore be said that the adequate amount of water and high pozzolanic reactivity were the reasons why 5% MIRHA paste has higher interfacial bond strength.

4.6.2 Interfacial Bonding Strength of Aggregate/Mortar with MIRHA 700

Figure 4.14 shows the interfacial bond strength between of aggregate/mortar with MIRHA at 700°C. From the result, bond strength of MIRHA mortar is significantly higher compared to control concrete. MIRHA mortar samples, 10% and 5% additions of MIRHA had slightly different bonding strength. Since the cement content was reduced by replacement of MIRHA, the lower hydration process was the reason of lower strength of 20% and 15% MIRHA mortar. It was found that 10% is the optimum level of replacement.

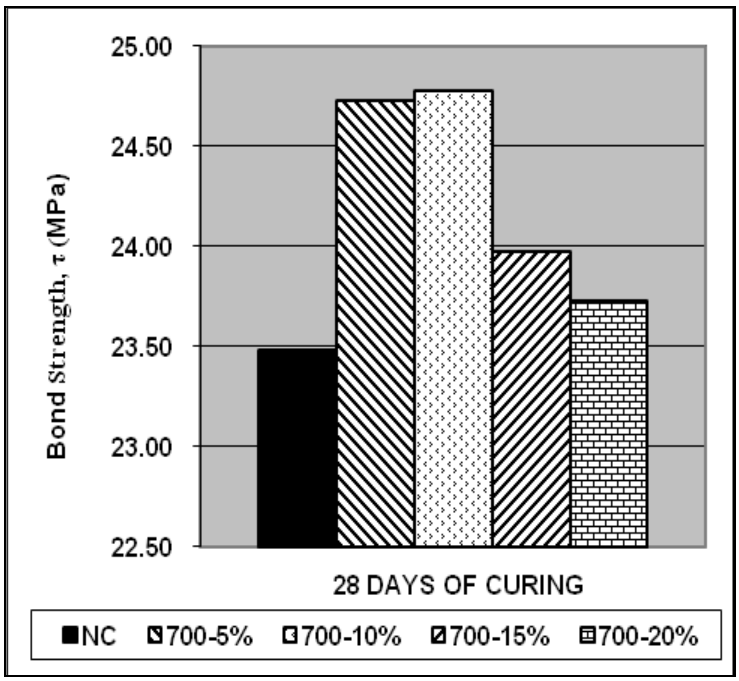

Figure 4.14 Interfacial Bond Strength of Aggregate/Mortar with MIRHA 700

4.6.3 Interfacial Bonding Strength of Aggregate/Mortar with MIRHA 600

From Figure 4.15, it also shows that the higher percentage of MIRHA inclusion into the pastes directly reduces the interfacial bond strength. It is due to the declining of cement content in the mix proportion that reduces the production of CSH gels to fill up the pore structure inside the concrete and creates water-filled space that affects the interfacial zone of aggregate/mortar.

Lower content of $Ca(OH)_2$ produced also affected the pozzolanic reaction with SiO_2. Therefore at 15% and 20% MIRHA concrete, interfacial bond strength was slower since there were larger amount of water-filled spaces left and fewer amounts of CSH gels produced. Compared to plain cement paste, 5% MIRHA had 2.4% higher bond strength then plain cement paste; meanwhile 10% MIRHA had 1.8% higher than plain cement paste. There is no significant difference of interfacial bond strength between 15% and 20% MIRHA concrete at 28 days. This is related to performance of hydration process and it is believed the hydration process was similar between the 5% and 10% MIRHA in which the difference is 0.3%.

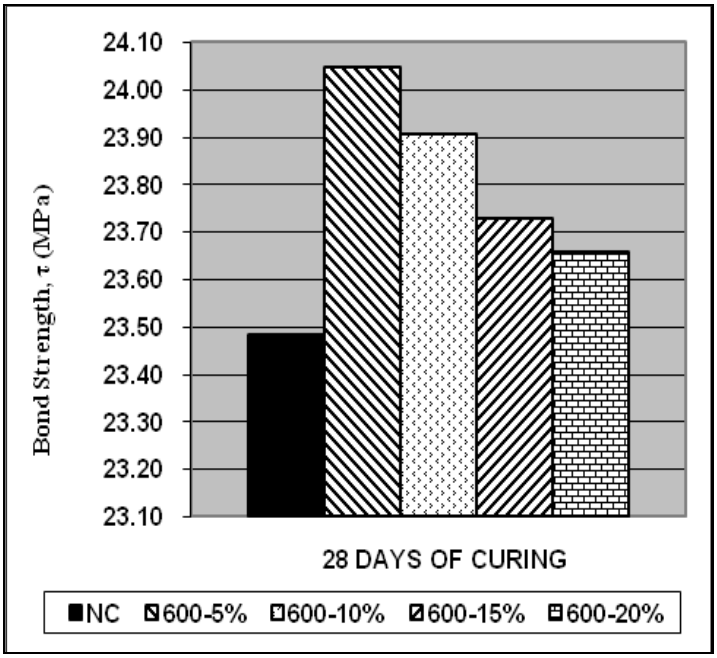

Figure 4.15 Interfacial Bond Strength of Aggregate/Mortar with MIRHA 600

4.6.4 Interfacial Bonding Strength of Aggregate/Mortar with SGR-RHA

Figure 4.16 presented the interfacial bond strength of aggregate/mortar without RHA and with SGR-RHA. The interfacial bond strength of concrete containing SGR-RHA was found to be lower than normal concrete without consideration of different percentages inclusion of SGR-RHA.

From the figure, SGR-RHA concrete shows that only 5% of inclusion gave a better performance compared to normal concrete while 10%, 15% and 20% inclusion of RHA leads the decreasing of interfacial bond strength compared to replacement at 5%. For the comparison, 5% replacement of SGR-RHA shows 1.51%, 10% replacement of SGR-RHA shows 1.36%, 15% replacement of SGR-RHA shows 0.6% and 20% replacement of SGR-RHA shows 0.15% higher than bond strength of normal specimen.

The contribution of SGR-RHA to the early bond strength is probably through improvement in packing, that is, action as a filler and improvement of the interface zone with the aggregate. On the other hand, in the present of alkalis; K_2O, the bond strength can be higher.

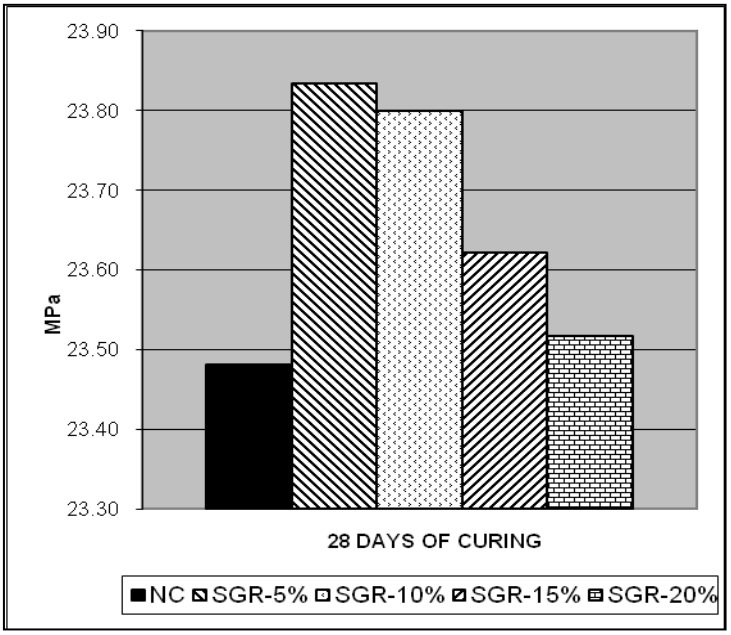

Figure 4.16 Interfacial Bond Strength of Aggregate/Mortar with SGR-RHA

4.6.5 Interfacial Bonding Strength of Aggregate/Mortar with SGM-RHA

Figure 4.17, shows the comparison of interfacial bond strength of aggregate/mortar for normal concrete and with SGM-RHA with optimum percentage (5%).

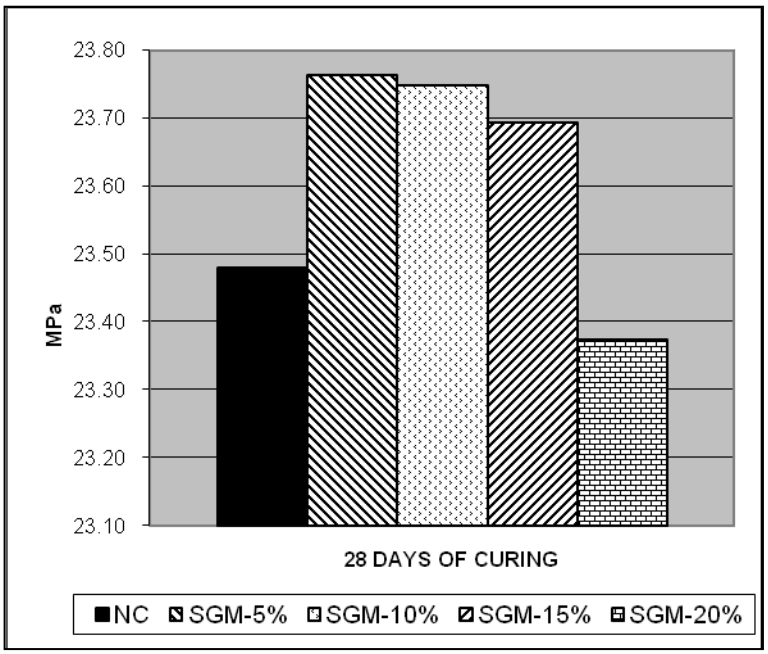

Figure 4.17 Interfacial Bond Strength of Aggregate/Mortar without RHA and with SGM-RHA

It can be seen that SGM-RHA has the optimum replacement at 5% which provides 1.2% better interfacial bond strength compared to normal concrete. From the result, bond strength of all SGM-RHA aggregate/mortar samples are significantly higher compared to control specimen but not including 20% replacement. The 5% replacement of SGM-RHA samples achieved interfacial bond strength performance 1.2% higher than control sample, SGM-RHA at 10% replacement achieved 1.14% higher than control sample, meanwhile SGM-RHA at 15% replacement shows 0.9% higher compared to the control sample.

It has been reveal from Figure 4.18 also that replacement of SGM-RHA at 20% to the concrete mixture did not absorbed water unlike MIRHA mixture and cause the mixture to be wet. It could be due to the characteristic of the ash which it replacement at 20% caused the mixture was able to bleeding and segregation. It is believed that effect of very high of surface area had made the SiO_2 could not interact sufficiently while the hydration process.

4.6.6 Interfacial Bonding Strength of Aggregate/Mortar of All Samples

Figure 4.18 shows the interfacial bond strength among of concrete samples. Based on the results, the interfacial bond strengths of all MIRHA pastes were remarkably higher compared to plain cement mortar while SGR-RHA and SGM-RHA show a slightly different from plain cement mortar.

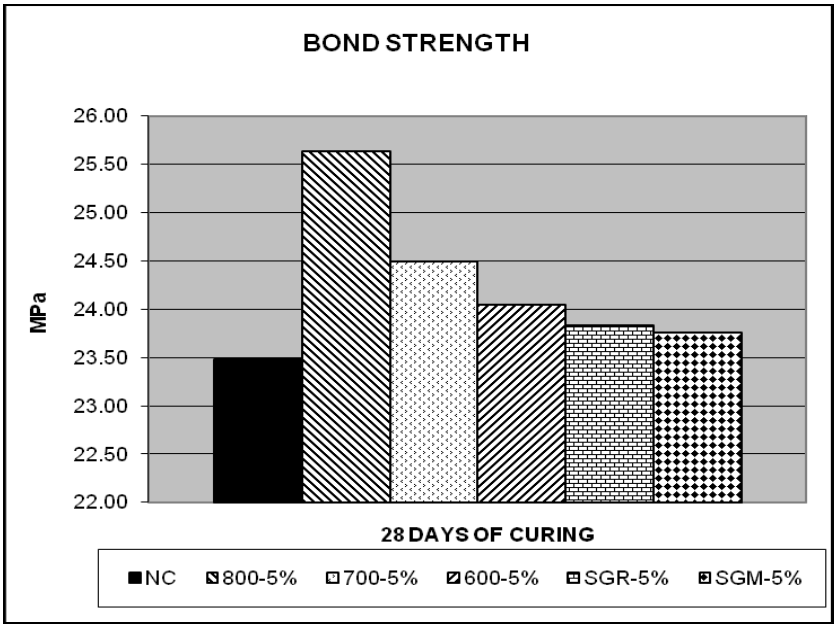

Figure 4.18 Interfacial Bond Strength of All Concrete Samples

The 5% inclusion of MIRHA burnt at 800°C in mortar paste shows the highest interfacial bond strength amongst the sample tested. This phenomenon occurred in all RHA mortar samples which are due to the declining of cement content in the mix proportion that reduces the production of C-S-H gels. These gels function are to fill up the pore structure beside the concrete and create water-filled space that affects the ITZ of aggregate/mortar. Low content of $Ca(OH)_2$ produced will affect the pozzolanic reaction with SiO_2. SGR-RHA and SGM-RHA samples had lower bond strength compared to MIRHA samples because there were large amount of water-filled spaces left and fewer amount of C-S-H gels produced.

However, it can be seen in the graph, even 10%, 15% and 20% replacement show the decreasing of bond strength, it still higher than bond strength of normal concrete.

It can conclude that all samples have optimum replacement at 5%. Based on previous result in previous chapter, one consequence of the high early reactivity of MIRHA, SGR-RHA and SGM-RHA is that the mix water is rapidly used up; in other words, self-desiccation takes place. In consequence, interfacial bond strength is much higher than with Portland cement alone.

4.7 Scanning Electron Microscope (SEM)

4.7.1 Interfacial Zone Thickness

Interfacial zone thickness of concretes is identified by conducting SEM Test. Interfacial zone is defined as the gap length between the aggregate and mortar matrix of the concrete. The test is conducted to compare the interfacial zone thickness in normal concrete to SGR-RHA, SGM-RHA and MIRHA concrete

Figure 4.19 shows the result obtained to identify interfacial zone thickness through SEM test. It could be noticed that 800°C is the optimum burning temperature that shows MIRHA 800 specimens depicting the small thickness of gap between cement paste and aggregate compared to normal cement paste.

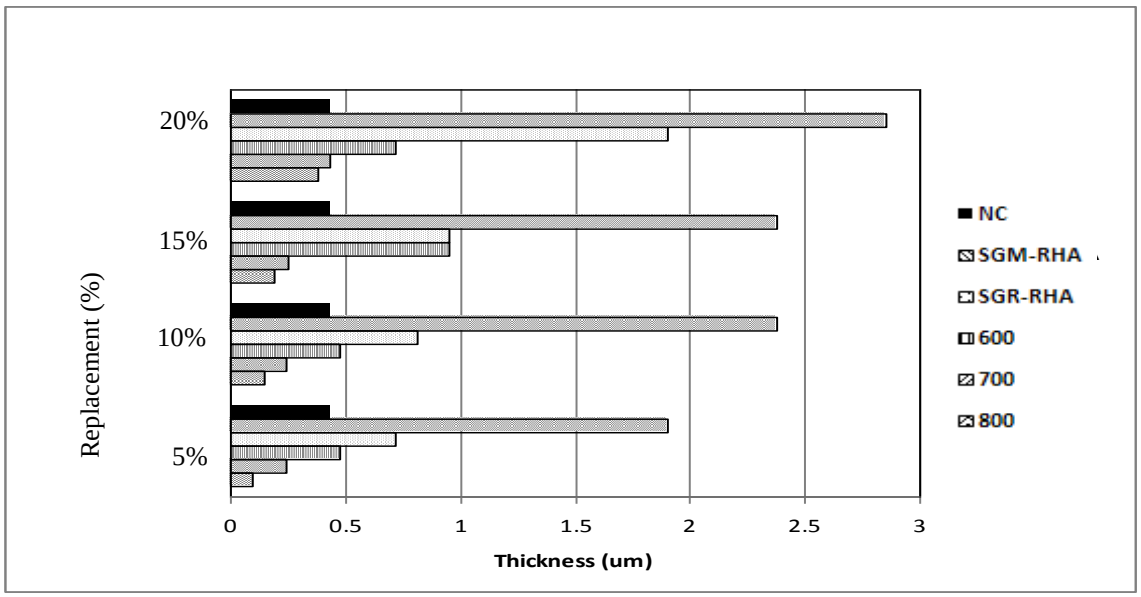

Figure 4.19: Interfacial Zone Thickness of NC, MIRHA, SGR-RHA and SGM-RHA Mortars.

It is due to the presence of MIRHA 800 that provides a denser interface by acting as filler and providing secondary hydration products. Meanwhile, the usage of super plasticizer increase the workability of the concrete by helping to deflocculates the cement and MIRHA particles, and reduction in the water content of the mix, as well as providing extra consistency.

From previous result of XRF, low crystalline intensity of MIRHA 800 had affected the process of cement hydration which resulted on a strong connectivity between cement paste and aggregate. The figure also displays that MIRHA 800 and MIRHA 700 show positive effects of MIRHA replacement on interfacial transition zone regardless of burning temperature. From the result, interfacial transition zone thickness of SGR-RHA and SGM-RHA concretes are bigger compared to normal concrete. Figures 4.20 to 4.25 show the SEM Images of the optimum replacement of each sample of MIRHA and RHA.

It can be seen from the images that the thickness between cement paste and aggregate become wider with replacement of MIRHA 700, MIRHA 600, SGR-RHA and SGM-RHA. The optimum percentage of replacement of each temperature was taken and compared with control specimen without MIRHA and RHA. From the research results, it revealed that burning RHA above 800°C will cause the crystalline state to occur. Once the crystalline state occurred, the material would convert to crystalline silica and lowered down the reactivity of the pozzolanic actions.

SGR-RHA and SGM-RHA samples had wider thickness of ITZ of all the percentages replacement. It can be conclude that the characteristic of the ash for both samples had affected the ITZ thickness. It is believed that the surface area and the fineness of the ash were the reason for the interruption of cement hydration process. Thus it produced insufficient amount of $Ca(OH)_2$ that made pozzolanic reaction did not to occur properly and lowered down the production of C-S-H gels. The C-S-H gels create water-filled space that affected the interfacial zone of aggregate or mortar. Besides that, C-S-H gels also have functions to fill up the pore structure inside the concrete. Therefore, less production of C-S-H gels led to lower mortar strength as there were a lot of pore structures in the concrete and made the interfacial thickness of the concrete increased.

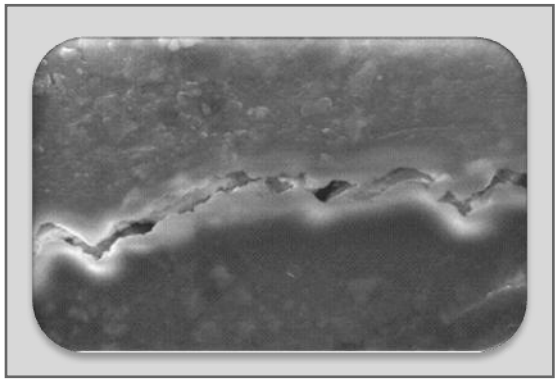

Figure 4.20 SEM Images of Control Concrete

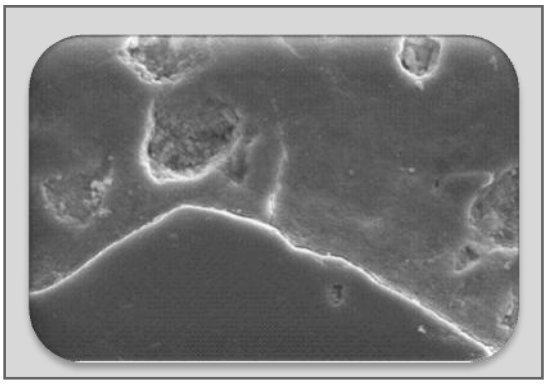

Figure 4.21 SEM Images of MIRHA 800-5%

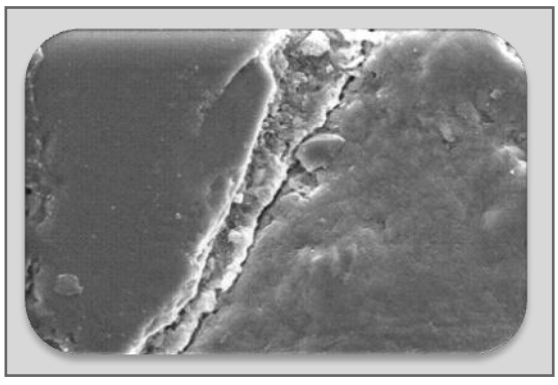

Figure 4.22 SEM Images of MIRHA 700-10%

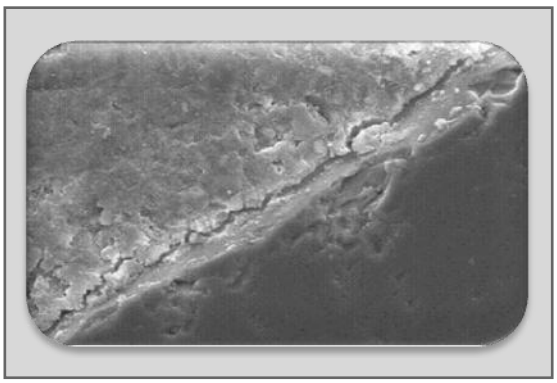

Figure 4.23SEM Images of MIRHA 600-5%

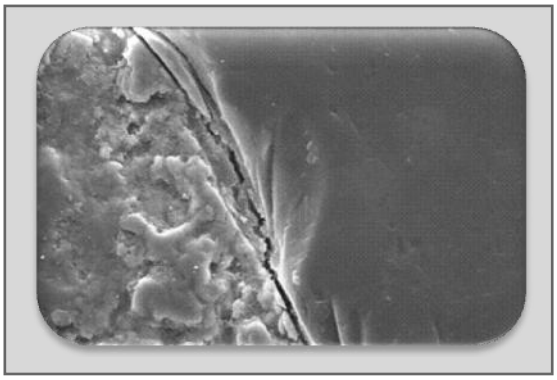

Figure 4.24 SEM Images of SGR-RHA-5%

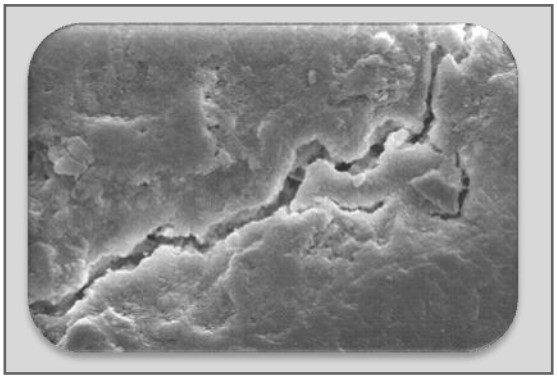

Figure 4.25 SEM Images of SGM-RHA-5%

4.7.2 Microcracking Thickness

Microcracking thickness is identified by conducting SEM Test where it defines the microcracking gap between the aggregate and mortar matrix in the concrete. Figure 4.26 shows the comparison of microcracking thickness of concrete without and with RHA. The comparisons are measured at different burning temperature and percentage of inclusion as well as SGR-RHA and SGM-RHA. From the results obtained, there is a noticeable difference between NC, MIRHA, SGR-RHA and SGM-RHA samples. MIRHA 800 without concern on percentage of replacement has low crack thickness compared to other specimens. It is believed that burning temperature and burning procedure can give a significant influence on the quality of the RHA.

As discussed on XRF result, burning RHA with high temperature and short time burning process produced RHA with high intensity of crystallinity. This type of RHA did not perform as a good as MIRHA where RHA could partially be converted to crystalline silica which did not react with $Ca(OH)_2$.

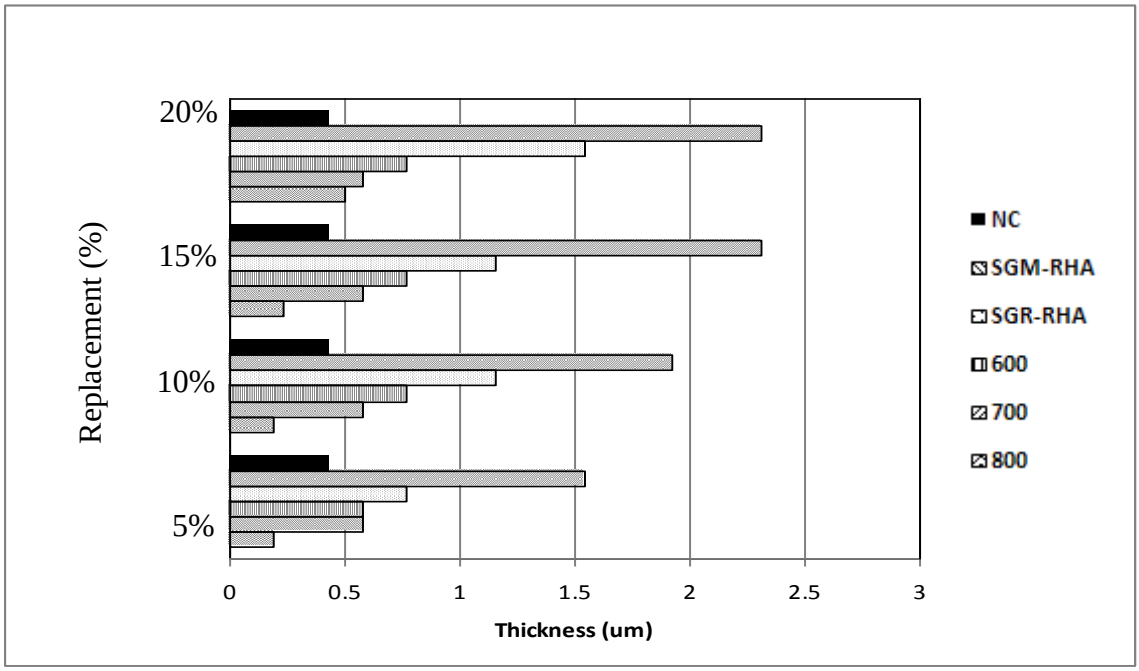

Figure 4.26 Microcracking Thickness of NC, MIRHA, SGR-RHA and SGM-RHA Mortars.

The SEM image of SGM-RHA and SGR-RHA revealed the circumstance. In addition, little pozzolanic reaction will lessen the strength and durability that can cause high crack thickness to the concrete. From the figure, it can be conclude that amongst all types of concretes, MIRHA 800 replaced into the concrete mix proportion have the ability to perform its function as a pozzolanic material and as a filler. The refinement in the structures could improve the weakness possessed by normal concrete paste. These improvements led to the higher compressive strength obtained by this MIRHA 800 with 5% replacement as previous results.

Comparing all types of samples, the inadequate amount of silica had made MIRHA 700 and MIRHA 600 concretes could not perform pozzolanic reaction effectively where the progress of hydration of cement can be determined by the amount of $Ca(OH)_2$. This phenomena had interrupted the cement hydration process to produce $Ca(OH)_2$. With insufficient amount of $Ca(OH)_2$, pozzolanic reaction could not occur properly and resulted in lower calcium silicate hydrate (C-S-H) gels being produced. Referring to the SEM images, Figures 4.27 to Figure 4.32 present the interfacial transition zone (ITZ) characteristic of all samples in terms of microcracking.

Meanwhile Figure 4.26, the optimum replacement of MIRHA 800 at 5% gives 0.193 μm thickness of ITZ while from figures it shows that there is no significant difference in microcracking thickness between all percentages of inclusion in MIRHA 700. It is because the performance of the hydration process. It is believed that the hydration process was similar between all percentages of inclusion in the MIRHA.

From the results, it presents that the 5% inclusion of MIRHA has the lowest value which is 0.578μm. Meanwhile the other percentages inclusions of MIRHA 600 give similar value which is 0.77 μm. It is believed that with lower burning temperature, the ability to extract the optimum amount of silica in rice husk is hampered and this in turn interrupted the cement hydration process to produce $Ca(OH)_2$. As a result, low content of $Ca(OH)_2$, lowered the pozzolanic reaction and the production of C-S-H gels that increased the microcracking thickness in RHA concrete samples.

Figures 4.31 and 4.32 reveal that among all concrete samples, the thickness of microcracking of SGR-RHA and SGM-RHA were different where there are much wider with those shown by MIRHA samples. It can be concluded that even RHA was burnt in a short time which to produce an amorphous ash, but apart from that, the temperature must be controlled since the result shows that high burning temperature can produce high of crystalinity of ash. The effect of crystallinity can be seen in the SEM images as shown below.

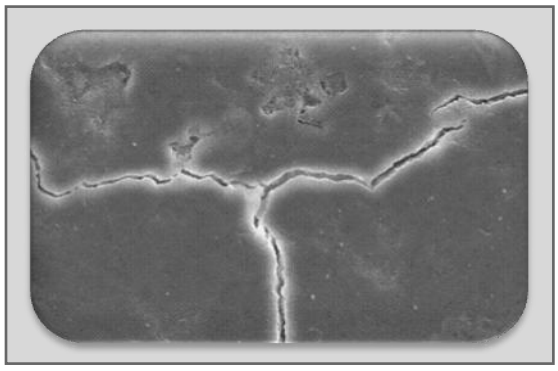

Figure 4.27 SEM Images of Control Concrete

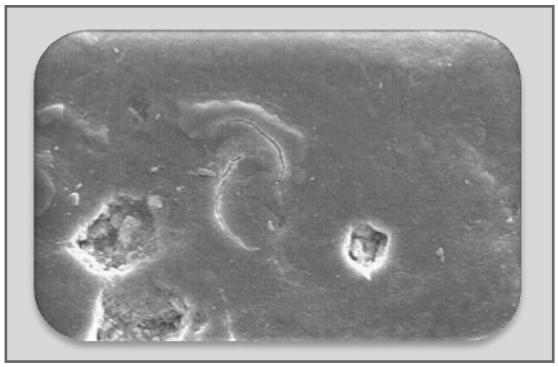

Figure 4.28 SEM Images of MIRHA 800-5%

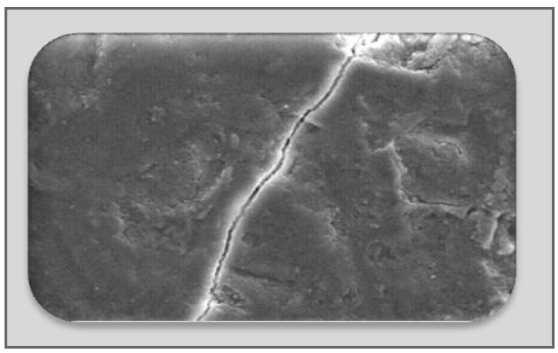

Figure 4.29 SEM Images of MIRHA 700-10%

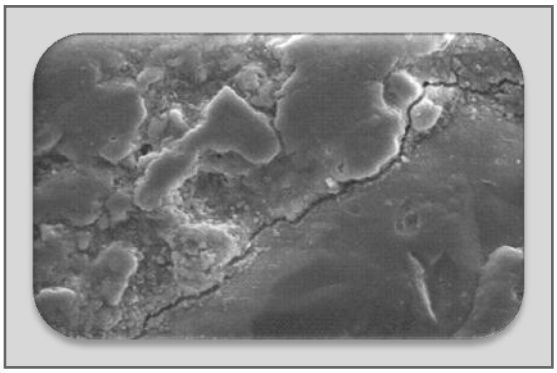

Figure 4.30 SEM Images of MIRHA 600-5%

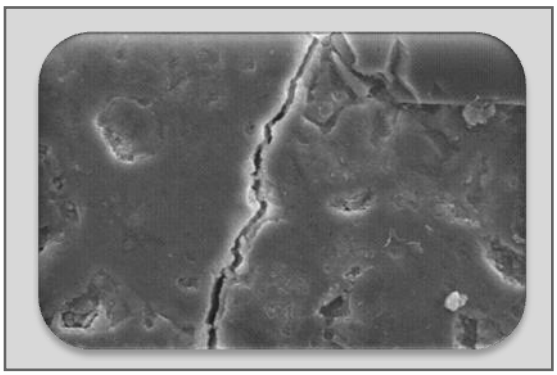

Figure 4.31 SEM Images of SGR-RHA-5%

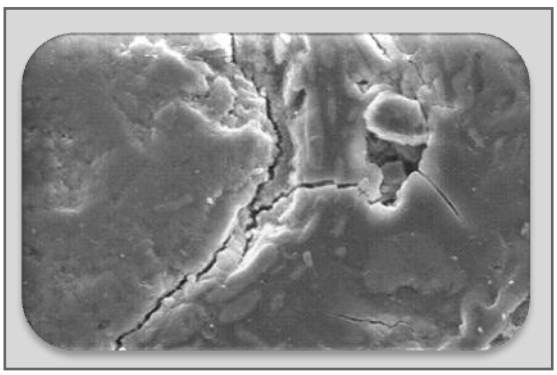

Figure 4.32 SEM Images of SGM-RHA-5%

CHAPTER V
CONCLUSIONS AND RECOMMENDATIONS FOR FUTURE RESEARCH

5.1 Conclusions

This research was carried out to identify the best burning procedure of rice husk, to obtain quality rice husk ash that can significantly improve the concrete properties. The utilization of Microwave Incinerated Rice Husk Ash (MIRHA) into the concrete mix proportions has given various effects to the concrete properties. The improvement of compressive strength, porosity and characteristic of ITZ, results of MIRHA concrete samples were influenced by the quality of MIRHA and mix proportion that were used. The following conclusions can be drawn from the study:

1. From three different burning methods, burning RHA by using microwave incinerator was found to be the best way to produce optimal output of RHA in terms of Si_2O quantity and quality.
2. From three different burning temperatures, 800°C produced MIRHA with optimum amount of Si_2O with high amorphousness compared to 700°C and 600°C. Meanwhile, SGR-RHA and SGM-RHA show that even Si_2O content was high, RHA concretes could not perform better compared to MIRHA concretes due to high content of crystalline in the ash.
3. Even at three days, MIRHA concretes are higher in terms of strength compared to NC (normal concrete). This research shows that burning MIRHA at 800°C, produce concrete with higher strength compared to 700°C and 600°C burning temperature, regardless of MIRHA percentage inclusion. Temperatures of 800°C revealed that addition of just 5% of MIRHA is the optimum percentage of cement replacement to produce concrete with good performance at early age and gained higher strength.

4. The porosity of MIRHA concretes are lower compared to Normal Concrete (NC) regardless of burning temperature of MIRHA. Meanwhile in other view, this research shows that burning MIRHA at 800°C, produce concrete with lower porosity compared to 700°C and 600°C burning temperature. Porosity of MIRHA concretes are found lower compared to SGR-RHA and SGM-RHA burnt at rice mills under high temperature.
5. Interfacial bond strength of aggregate/mortar with MIRHA is higher compared to plain cement mortar regardless of burning temperature of MIRHA. Specifically, 5% MIRHA 800 replacement with cement and addition of superplasticizer to the mortar produced a thinner interfacial zone than the plain cement mortar and both of SGR-RHA and SGM-RHA cement mortars. This stems from the fact that MIRHA densifies the microstructure by acting as a filler as well as providing a secondary hydration products, while SP provides deffocculation of the cement and MIRHA particles, as well as extra flow capability to the mix so that better packing would be possible.
6. The thickness of ITZ of MIRHA aggregates/mortars are lower compared to SGR-RHA and SGM-RHA aggregates/mortars regardless of burning temperature of MIRHA. Clearly, this research shows that burning MIRHA at 800°C, produce mortar with lower thickness of ITZ compared to 700°C and 600°C burning temperature. This research shows that burning MIRHA at 800°C and with 5% of inclusion in aggregate/mortar, produce aggregate/mortar with lower thickness of ITZ compared to all samples.
7. Optimum mix proportion that was obtained from this research was based on the compressive strength, porosity, aggregate/mortar bonding strength and ITZ characteristic of MIRHA concrete samples. It comprises of :

Burning temperature	: 800°C
OPC Type 1	: 451.25 kg/m^3,
MIRHA	: 23.75 kg/m^3 (5% replacement)
Water	: 213.75 kg/m^3
Fine aggregates	: 607.25 kg/m^3, and
Coarse aggregates	: 1127.75 kg/m^3.
w/c	: 0.45

5.2 Recommendations for Future Research

To explore the potential of MIRHA application in construction industries, the following works are recommended to analyze the concrete properties containing MIRHA more comprehensively:

1. This research observed the effect of MIRHA on dry and wet concrete with the slump value kept between 30 – 60 mm. As the amount of water can affect the performances of MIRHA, it is recommended that wider range of H_2O content is taken into consideration.
2. For finest of MIRHA particle, this research observed the effect of MIRHA with one range of size. Grinding the cement more finely will result in a more rapid increase in strength. With varies finest of MIRHA, the consequence of particle can be examined thus assessment on the filler effect can be observed.
3. In the case of porosity, standard practice of curing for 28 days is found to be adequate. Prolonged curing up to 90 days is suggested for the point of view of improving the resistance to water absorption and interfacial transition zone characteristic.
4. The effect of MIRHA on the reinforcement steel inside the concrete need to be observed as the durability of reinforced concrete constructions leading to an enhanced design life.

Hence, commercialization of MIRHA needs to be considered. There are a lot of findings and studies show MIRHA is a good material as a cement replacement material. To this extent, the utilization of MIRHA can be exploited.

REFERENCES

[1] N. Yelcin, V. Sevinc, *Studies on silica obtained from rice-husk,* Ceramics International 27, pp. 219-224, 2001.

[2] Bronzeoak Ltd., "Rice Husk Ash Market Study," EXP 129, DTI/Pub. URN 03/668, 2003.

[3] Business Monitor International, "Malaysia Agribusiness Report Q3," 2010.

[4] United Nations Industrial Development Organization (with Govt. of Australia), Vienna, *Rice-Husk Ash Cement,* 1984.

[5] D. F Houston, *Rice Hulls in Rice: Chemistry and Technology,* American Association Cereal Chemists, 1972, pp. 301-352.

[6] S. K. Chopra "Utilisation of rice husk for making cement and cement like binders, Rice husk ash cement," in *Proc UNIDO/ESCAP/RCTT/PCSIR Joint workshop, Peshawar, Pakistan and Bangalore,* India, 1979, pp. 135-149.

[7] A. Singh, K. Das and D. K. Sharma, "Production of Reducing Sugars from Bagasse and Rice Husk Ash by Acid Hydrolisis," Agriculture Wastes, 9: 131-145, 1984, vol. 2.

[8] C. L. Hwang, and S. Chandra, "The Use of Rice Husk Ash in Concrete," in *S.Chandra, Waste Materials Used in Concrete Manufacturing (pp. 184-234),* William Andrew Pub.1996.

[9] C. L. Hwang, and D. S. Wu. Properties of Cement Paste Containing Rice Husk Ash. *ACI Mterials Journal SP-114* (Editor: V. M.Malhotra), pp. 733-765. 1989.

[10] C. L. Hwang and S. Chandra, "The Use of Rice Husk Ash in Concrete," *Waste Materials Used in Concrete Manufacturing,* Edited by S. Chandra, Noyes Publications, USA, 1997, pp. 198.

[11] K. Kartini, B. H. Mahmud, M. S. Hamidah, "Improvement on Mechanical Properties of Rice Husk Ash Concrete with Superplasticizer," presented at International Conference on Construction and Building Technology (ICCBT), 2008.

[12] I. A. Rahaman and F. L. Riley. (1989). The control of morphology in silicon nitride powder prepared from rice husk. *J. Euro. Ceram Soc.5*, pp. 11-22.

[13] S. Chandrasekhar, K. G. Satyanarayana, P. N. Pramada, P. Raghavan. (2003). Review Processing, properties and applications of reactive silica from rice husk-an overview. *Journal of Material Science. vol. 3*, pp. 3159-3168.

[14] Amitabha Kumar. "Mineral admixture in cement and concrete," in *Rice husk ash based cements, vol.4,* Central glass and ceramic research institute Jadavpur, Calcutta 700 032, India. 1999.

[15] A. Dass and M. Rai. "Prospects and problems in the production of cementitious materials from rice husk," in *Rice Husk Ash Cement,* 1979, pp. 49-56.

[16] A. Kumar, D. K. Das and G. Banerjee. (1989). Internal report on utilization of rice husk ash for cost effective builidings material, CGCRI, Calcutta, India.

[17] R. Jauberthie, F. Rendell, S. Tamba, I. Cisse. (2000). Origin of the pozzolanic effect of rice husks. *Construction and Building Materials, vol.24(11).*

[18] M. A. Hamad, I. A Khattab. (2001). Effect of the combustion process on the structure of rice hull silica. *Thermochimica Acta,vol. 48(3).*

[19] E. Effstathiadis. *Greek Concrete of Three Millenias*. Hellenic Ministry of Public Works, Athens. 1978.

[20] *Standard Specification for Coal Fly Ash and Raw or Calcined Natural Pozzolan for Use in Concrete,* ASTM Standard C168, 08a, ASTM International, West Conshohocken, PA, DOI: 10.1520/C0618-08, 2008.

[21] S. Chandrasekhar, P. N. Pramada, P. Raghavan, K. G. Satyanarayana. (2002). Microsilica from rice husk as a possible substitute for condensed silica fume for high performance concrete. *Journal of Materials Science Letters. vol. 21,* pp. 1245-1247.

[22] *Catalogue of Elkem Microsilica® Grade 920,* Production and Use, C1-02, February 2000.

[23] *Concrete admixtures handbook 2nd ed.*, V. S. Ramachandran, Noyes Publications, USA, 1995.

[24] M. N. Al-Khalaf, A. Hana Yousif. (November, 1984). Use of rice husk ash in concrete. *International Journal of Cement Composites and Lightweight Concrete. vol. 6, Issue 4,* pp. 241-248.

[25] J. D. Cook. (1986). "Rice husk ash," in R. N. Swamy, editor, Concrete technology and design.*Cement replacement materials. vol. 3,* pp. 171-95.

[26] A. A. Boating, D.H. Skeete. (1990). Incineration of rice hull for use as a cementitious materials; the Guyana experience. *Cement Concrete Res. vol. 20,* pp.795-802.

[27] J. James, M. Subba Rao. (1986). Silica from rice husk through thermal decomposition. *Thermochim Acta (97).* Elsevier Science. Amsterdam. pp. 329-36.

[28] K. Ganesan, K. Rajagopal, K. Thangavel. (2007). Rice husk ash blended cement: Assessment of optimal level of replacement for strength and permeability properties of concrete. *Construction and Building Materials. vol. 22(8),* pp. 1675-1683.

[29] K. Ankra, "Studies of Black Silica Produced under Varying Conditions," Ph.D. dissertation**,** University of California at Berkeley, 1975.

[30] R. Smith, *Rice Husk Ash Cement: Progress in development and application,* Intermediate Technology Publication Limited, London, 1984.

[31] M. H. Zhang, R. Lastra, V. M. Malhotra. (1996). Rice-husk ash paste and concrete: Some aspects of hydration and the microstructure of the interfacial zone between the aggregate and paste. *Cement and Concrete Research*. *vol. 26(6).*

[32] S. Chakrabarti, P. Chakrabarti, S. Saha, and S. Datta, *Inst.Chem. Eng. Symp. Ser*. 105, 1988, pp. 339.

[33] Rice Engineering Supply Co. Ltd**.** Modern Rice Milling, Corn Paddy Drying System, Parboiled Paddy Drying Plant. 2008.

[34] Alberto R. Dalusung III, John Cesar B. Santos, La Suerte Rice Mill Cogeneration Project: A PILOT Case for the Philippines, Electricity Supply Industry in Transition: Issues and Prospect for Asia. 14-16 January 2004.

[35] PRM Energy System Inc. Biomass Gassification Technology, 1987-1993.

[36] Bentech. Operation & Maintenance manual for Microwave Incinerator. 2006.

[37] Andri Kusbiantoro, "The Effect Of Microwave-Incinerated Rice Husk Ash (MIRHA) On Concrete Properties Studies of Black Silica Produced Under

Varying Conditions," M.S. thesis, Civil Engineering Department, Universiti Teknologi Petronas, 2007.

[38] C. M. Neubauer , H. M. Jennings, and E. J. Garboczi. (1996). A Three-Phase Model of the Elastic and Shrinkage Properties of Mortar. *Advanced Cement Based Material. vol. 4,* pp. 6-20.

[39] *X-Ray Fluorescence Spectroscopy*, Amptek, Bedforf, MA.USA. 2002.

[40] *Chemical analysis of refractory products by XRF*, BS EN 12677, 2003.

[41] Karl Wirth. (July, 2009). X-Ray Fluorescence (XRF). Macalester College and Andy Barth, Indiana University~Purdue University, Indianapolis.

[42] Limnological Research Center Core Facility. (2004). X-Ray Diffraction.

[43] G. B. Arehart, *Introduction to X-Ray Diffraction.* Department of Geological Sciences MS 172, University of Nevada-Reno.

[44] *Siliceous Ashes and Hydraulic Cements Prepared Therefrom*, by Mehta, P. K. (August, 1978). *US Patent. 4105459.*

[45] D. G. Nair, K. S. Jagadish, A. Fraaij. (2006). Reactive Pozzolanas from Rice Husk Ash: An Alternative to Cement for Rural Housing. *Cement and Concrete Research. vol. 36.* pp 1062-1071.

[46] Josh Klesel, Scott Chumbley. (January, 2003). *Welcome to the World of Scanning Electron Microscopy*. Iowa State University, Material Science and Engineering Department. Available: http://mse.iastate.edu/microscopy/home.html

[47] R. Jauberthiea, U. F. Rendella, S. Tambab, I. Cisse. (2000). Origin of the Pozzolanic Effect of Rice Husks. *Construction and Building Materials. vol. 14,* pp 419-423.

[48] Q. Yu, K. Sawayama, S. Sugita, M. Shoya, Y. Isojima. (1999). The Reaction Between Rice Husk Ash and $Ca(OH)_2$ Solution and The Nature of Its Product. *Cement and Concrete Research 29,* pp 37-43.

[49] N. L. M. Kamal, M. F. Nuruddin and N. Shafiq, "The Influence of Burning Temperatures and Percentage Inclusion of Microwave Incinerated Rice Husk Ash (MIRHA) on Normal Strength Concrete," presented at International Conference on Construction and Building Technology (ICCBT), 2008.

[50] P. K. Mehta, (1992). *Rice Husk Ash-A Unique Supplementary Cement Material*. Advances in Concrete Technology, Ed. By Malhotra, CANMET, Ottawa, Canada,

[51] O. A. Kayyali. (1987). Porosity of concrete in relation to the nature of the paste—aggregate interface. *Materials and Structures vol. 20(1),* pp. 19-26.

[52] A. U. Nilsen and P. J. M. Monteiro. (1993). A three-phase model of the elastic and shrinkage properties of mortar. *Advanced Cement Based Materials. vol. 4(1),* pp. 6-20.

[53] M. D. Cohen, A. Goldman and W. F. Chen. (1994). The role of silica fume in mortar: Transition zone versus bulk paste modification. *Cement and Concrete Research vol. 24(1),* pp. 95-98.

[54] E. J. Garboczi, L. M. Schwartz and D. P. Bentz. (1995). Modelling the Influence of the Interfacial Zone on the Conductivity and Diffusivity of Mortar. *Advanced Cement Based Materials. vol. 2(5),* pp. 169-181.

[55] K. L. Scrivener, A. Bentur and P. L. Pratt. (1988). *Quantitative Characterization of the Transition Zone in High Strength Concrete. Advances in Cement Research. vol. 1(4),* pp. 230-327.

[56] D. P. Bentz, P. E. Stutzman and E. J. Garboczi, (1992). Experimental and Simulation Studies of the Interfacial Zone in Concrete. *Cement and Concrete Research* vol. 22(5), pp. 891.

[57] A. Goldman, and A. Bentur. (September, 1989). Bond Effects in High-Strength Silica-Fume Concretes. *ACI Materials Journal. vol. 86(5),* pp. 440-447.

[58] A. Goldman and A. Bentur. (July, 1993). The influence of Microfillers on Enhancement of Concrete Strength. *Cement and Concrete Research vol. 23(4),* pp. 962-972.

[59] A. Bentur, M. D. Cohen. (March, 2005). Effect of Condensed Silica Fume on the Microstructure of the Interfacial Zone in Portland Cement Mortars. *American Ceramic Society. vol. 70(10),* pp. 738-743.

[60] A. Bentur, A. Goldman and M. D. Cohen. (1988). The contribution of the Interfacial Zone to the Strength of High Quality Silica Fume Concretes. *Materials Research Society. vol. 114,* pp. 97-103.

[61] K. L. Scrivener, A. Bentur, P. L. Pratt. (October, 1988). Quantitative Characterization of the Transition Zone in High Strength Concretes. *Advances in Cement Research. vol. 1(4),* pp. 230-237.

[62] Sinan Caliskan. (May, 2003). Aggregate/mortar interface: influence of silica fume at the micro- and macro-level. *Cement and Concrete Composites. vol. 25(4-5),* pp. 557-564.

[63] A. M. Neville, (1995). *Properties of Concrete*, Pearson Education Limited, England.

[64] Masao Kuroda, Tomohide Watanabea and Nariaki Terash. (February, 2000). Increase of Bond Strength at Interfacial Transition Zone by the Use of Fly Ash. *Cement and Concrete Research. vol. 30(2),* pp. 253-258.

[65] *Testing Aggregates. Method for Determination of Particle Size Distribution. Sedimentation Test,* BS 812-103.2, 1989.

[66] *Mixing water for concrete - Specification for sampling, testing and assessing the suitability of water, including water recovered from processes in the concrete industry, as mixing water for concrete,* BS EN 1008, 2002.

[67] *Cement. Composition, specifications and conformity criteria for common cements,* BS EN 197-1, 2000.

[68] Cement Quality, *Cement Industries of Malaysia Berhad,* 2009, Available: http://www.cima.com.my/cement_quality.php

[69] *Admixtures For Concrete, Mortar And Grout. Concrete Admixtures. Definitions, Requirements, Conformity, Marking And Labeling,* BS EN 934-2. 2001.

[70] *Testing concrete. Methods for mixing and sampling fresh concrete in the laboratory,* BS 1881-125. 1986.

[71] *Testing fresh concrete. Slump test,* BS EN 12350-2, 2000.

[72] *Testing hardened concrete. Making and Curing Specimens for Strength Tests,* BS EN 12390-2, 2000.

[73] *Standard Test Method for Determination of Relative X-ray Diffraction Intensities of Faujasite-Type Zeolite-Containing Materials,* ASTM D3906-03, 2008.

[74] *Testing Hardened Concrete. Compressive Strength Of Test Specimens,* BS EN 12390-3, 2002.

[75] *Absorption of water by immersion under vacuum, Materials and Structures, Research and Testing. No. 101,* RILEM, CP113, 1984.

[76] K. M. Lee, O. Buyukozturk, A. Oumera. (1992). Fracture Analysis of Mortar-Aggregate Interfaces in Concrete. *Journal of Engineering Mechanics, ASCE. vol. 118(10),* pp. 2031-2047.

[77] W. A. Tasong, C. J. Lynsdale, J. C. Cripps (1998). Aggregate-cement Paste Interface. II. Influence of Aggregate Physical Properties. *Cement Concrete Res. vol. 28(10),* pp. 1453-1465.

[78] K. Mitsui, Z. Li, D. A. Lange, S. P. Shah, (1992), "A study of properties of the paste-aggregate interface", *Proceedings of International Conference on Interfaces in Cementitious Composites,* RILEM Proceedings 17, France, pp.119-28.

[79] S. Caliskan, B. L. Karihaloo, B. I. G. Barr (2002). Study of Rock Mortar Interfaces. Part II: Strength of Interface. *Mag Concrete Res. vol. 54,* pp. 449-461.

[80] *Standard Practice for Scanning Electron Microscope Beam Size Characterization,* ASTM E986-04, 2010.

[81] Andri Kusbiantoro, "The effects of microwave incinerated rice husk ash (MIRHA) on concrete properties," present at National Postgraduate Conference, Universiti Teknologi Petronas, 2008.

[82] M. F. Nuruddin, A. Kusbiantoro, N. Shafiq, "Microwave Incinerated Rice Husk Ash (MIRHA) and it's Effects on Concrete Strength," presented at the 3rd IMS International Conference on Application of Traditional and High Performance Materials In Harsh Environments, Sharjah, (2008).

[83] A. M. Fadzil, M. J. Megat Azmi, A.B. Badrol Hisyam and M. A. Khairun Azizi, "Engineering Properties of Ternary Blended Cement Containing Rice Husk Ash and Fly Ash as Partial Cement Replacement Materials," presented at the International Conference on Construction and Building Technology (ICCBT), 2008.

APPENDIX A

Technical Specification for Microwave Incinerator Model Bentech Inc-21 [36].

ITEM			DESCRIPTION
A	**GENERAL DESCRIPTION**		
	i)	Manufacturer	Pollution Engineering Sdn Bhd
	ii)	Model	BENTECH INC-21
	iii)	Capacity	1 m^3 Chamber
	iv)	Type of Waste	Paddy Husk
	v)	Overall Dimension (m)	2.3 (H) x 4.0 (W) x 4.0 (L)
	vi)	Operating Temperature	800°C
	vii)	Emission & Ash Control System	Ceramic Filter
	viii)	Combustion Control	Temperature Controller
	ix)	Mode of Operation	PLC with Manual Overwrite
	x)	Mode of Loading	Manual
	xi)	Mode of Waste Ash Removal	Manual
B	**KILN CHAMBER**		
1	**Body Casing**		
	i)	Material and Thickness	SS 304 Plate Thickness 4.5 mm – 5.0 mm
	ii)	Support and Thickness	SS 304 Angle Iron 3 inch x 3 inch x t5.0 mm and above
2	**Charging Door**		
	i)	Dimension (mm) Big Door	580 x 455
	ii)	Dimension (mm) Small Door	315 x 315

C	**MICROWAVE INCINERATOR**			
	i)	Type	Air Cooled Magnetron	
	ii)	Manufacturer/Model	Pollution Engineering Sdn Bhd/ MG-AIR 2450-1100	
	iii)	Country of Origin	Malaysia	
	iv)	Power Rating (l/hr)	1100 W	
D	**THERMOCOUPLE**			
	i)	Length (mm)	300	450
	ii)	Type	In-Connel	
	iii)	Manufacturer/Brand	IPSH Sdn Bhd	
	iv)	Country of Origin	Malaysia	
	v)	Temperature Range	Up to 1600°C	
E	**SUPPLY AIR BLOWER**			
	i)	Type	TSB 50	
	ii)	Manufacturer/Brand	Fu-Tsu	
	iii)	Country of Origin	Taiwan	
	iv)	Motor rating	1.5 KW	
	v)	Air Capacity (m^3/min)	Not less than 1.87 m^3/min	
F	**CERAMIC FILTER**			
	i)	Type	CERAFIL XS-1000	
	ii)	Manufacturer/Brand	CERAFIL	
	iii)	Country of Origin	United Kingdom	
	iv)	Surface Area (m^2)	0.19	
G	**INDUCED DRAFT FAN**			
	i)	Type	HFD 3242 T	
	ii)	Manufacturer/Brand	Maxis Fan	
	iii)	Country of Origin	Malaysia	
	iv)	Motor Rating	4 HP	
	v)	Air Capacity (m^3/min)	Not less than 0.15 m^3/sec	

H	**AIR COMPRESSOR**		
	i)	Type	TS 05 120 H
	ii)	Manufacturer/Brand	ELGI
	iii)	Country of Origin	India
	iv)	Motor Rating	5 HP
	v)	Air Capacity (m^3/hr)	Not less than 24.6 m^3/hr at 10 kgf/cm^2
I	**CONTROL PANEL**		
	i)	Enclosure	IP54
	ii)	Model of Operation	Programmable Logic Control (PLC)
	iii)	Type of PLC	Omron or equivalent
	iv)	Type of Cubicle	MERLIN GERLIN
	v)	Type of Contractor	TELEMECANIQUE
	vi)	Type of Starter	TELEMECANIQUE
	vii)	Touch Screen	GT21 4.7 Inch Panasonic
J	**WIRING WORKS**		
	i)	Type of Wiring	PVC
	ii)	Type of Conduit/Cable Tray	Galvanized Conduit